Reconnection Remnants in the Magnetic Cloud of October 18-19, 1995: A Shock, Monochromatic Wave, Heat Flux Dropout and Energetic Ion Beam

Michael R. Collier, A. Szabo, W. Farrell, J.A. Slavin, R.P. Lepping,
R. Fitzenreiter and B. Thompson
Space Sciences Directorate, NASA/GSFC, Greenbelt, Maryland

D.C. Hamilton and G. Gloeckler
University of Maryland, College Park

G.C. Ho
Applied Physics Laboratory, The Johns Hopkins University, Laurel, Maryland

P. Bochsler
University of Bern, Switzerland

D. Larson
University of California, Berkeley

L. Ofman
Laboratory for Astronomy and Solar Physics, Raytheon ITSS and NASA/GSFC, Greenbelt, Maryland

date: 6 February 2000

Abstract. Evidence is presented that the WIND spacecraft observed particle and field signatures on October 18-19, 1995 due to reconnection near the footpoints of a magnetic cloud (i.e., between 1 and 5 solar radii). These signatures include (i) an internal shock traveling approximately along the axis of the magnetic cloud, (ii) a simple compression of the magnetic field consistent with the footpoint magnetic fields being thrust outwards at speeds much greater than the solar wind speed, (iii) an electron heat flux dropout occurring within minutes of the shock indicating a topological change resulting from disconnection from the solar surface, (iv) a very cold 5 keV proton beam and (v) an associated monochromatic wave. We expect that, given observations of enough magnetic clouds, Wind and other spacecraft will see signatures similar to the ones reported here indicating reconnection. However,

these observations require the spacecraft to be fortuitously positioned to observe the passing shock and other signatures and will therefore be associated with only a small fraction of magnetic clouds. Consistent with this, a few magnetic clouds observed by Wind have been found to possess internal shock waves.

1. Introduction

Magnetic clouds, a subset of interplanetary ejecta characterized by strong magnetic fields which exhibit a smooth, large rotation and low proton temperatures, are currently of great interest in part because of their association with coronal mass ejections (CME's) and because of their magnetospheric impact [*Burlaga et al.*, 1981; *Laakso et al.*, 1998; *Moore et al.*, 1999]. Magnetic clouds typically expand at about half the Alfvén speed and, due to their adiabatically decreasing magnetic field, are expected to disappear somewhere between 2 and 12 AU [*Osherovich et al.*, 1993]. With the fleet of satellites at 1 AU resulting from the International Solar-Terrestrial Physics (ISTP) program, magnetic cloud observations from solar origin through geomagnetic effect are now possible [e.g., *Fox et al.*, 1998].

The large-scale geometry of magnetic clouds is well-described by a force-free magnetic field represented by a set of helical field lines confined to a flux tube (flux rope) [*Burlaga*, 1995; *Wu et al.*, 1995; *Low and Hundhausen*, 1995] or flux tubes (flux ropes) [*Osherovich et al.*, 1999]. However, there appear to be smaller-scale physical processes occurring within magnetic clouds [*Christon et al.*, 1998; *Takeuchi et al.*, 1998].

Because magnetic cloud footpoints are frequently still attached to the Sun, we might expect to observe signatures on magnetic cloud field lines of time-dependent processes in the lower corona. One such time-dependent process is magnetic re-

connection which effects the disconnection of the footpoints [*Gosling et al.*, 1995]. Indeed, *Gosling* [1990] posits this as the basic process by which interplanetary flux ropes are formed.

2. The October 1995 Cloud

One example of a well-studied magnetic cloud was observed by the Wind spacecraft on October 18-19, 1995. An overview of the magnetic field and plasma parameters during this time is shown in Figure 1. The first three panels display Wind magnetic field data from the Magnetic Field Investigation (MFI) [*Lepping et al.*, 1995] with the upper panel showing the magnetic field magnitude in nanoteslas on a logarithmic scale (see Fig. 1 of Lepping *et al.* [1995] for a linear scale). The next two panels show in degrees the magnetic field angle out of the ecliptic plane, θ, and in the ecliptic plane, ϕ (with 0° pointing towards the Sun). The interior of the cloud is indicated by the two headed arrow between the vertical lines. Although there is some ambiguity about the location of the back of the cloud, it does not bear on this analysis, so we have only indicated one of the possible boundaries [*Lepping et al.*, 1997].

This cloud has been fit using a force-free "constant α" helical flux rope model resulting in cylindrical Bessel functions:

$$B_\phi = B_0 J_1(\alpha r) \tag{1}$$

$$B_z = B_0 J_0(\alpha r), \tag{2}$$

where B_ϕ and B_z are the azimuthal and axial fields, respectively, B_0 is the central field, r is the distance from the cloud axis, and α is a constant relating the current and magnetic field ($\alpha \mathbf{B} = \nabla \times \mathbf{B}$) [*Priest*, 1987].

The fitting result was awarded a rating of "1: excellent" on the subjective Lepping quality scale. This scale includes the ranks 1 for "excellent", 2 for "good", 3 for "poor" and "cl" for "cloud-like" indicating that the helical flux rope fitting is unlikely to be successful for any reasonable model. Of 34 magnetic clouds identified by Lepping using Wind data from 1995-1998 (including the October 1995 cloud), 13 were rated "excellent" (1), 15 were rated "good" (2), 5 were rated "poor" (3) and 1 was rated "cloud-like" (cl), so that in terms of fit quality, this cloud is in about the upper one-third.

Note that the magnetic field strength during the cloud interval is considerably higher than typical interplanetary values at 1 AU. Although there is no dramatic change in ϕ, the angle θ rotates steadily from pointing below to pointing above the ecliptic. The internal shock occurs slightly before 1800 UT and manifests as a significant jump in the magnetic field magnitude although the angles θ and ϕ remain largely unaffected.

The SWE density, thermal speed, and solar wind speeds are shown in the bottom three panels [*Ogilvie et al.,* 1995]. At the time of the internal shock, the density, thermal speed, and solar wind speed all abruptly increase, so that this internal shock has the characteristics of a typical fast forward MHD interplanetary shock. Lepping *et al.* [1997] refer to this as a "shock-in-formation," a compression still steepening into a shock, or a shock-like structure which seems to compress the magnetic field. We will simply refer to it as a shock. The magnetic field direction, as illustrated in Fig. 1, shows little change as the shock ramp passes Wind. Hence, it appears to be a perpendicular shock. The field is undergoing simple compression.

In addition, *inside* this magnetic cloud and just downstream of the interplanetary shock an unusually monochromatic wave of about one second period was

observed. Data from the Wind/MASS instrument show that at the time of this wave there was a very cold 5 keV proton beam present, and energetic electron pitch angle data from the Wind/SWE instrument show that all these unusual observations were associated with a topology change. This time period within the October 18-19, 1995 magnetic cloud is the subject of this paper.

A similar type of wave activity has been observed by Lucek and Balogh [1997] in Ulysses data. However, the period of these waves was about three seconds, and they lasted for about 3.5 minutes whereas the wave discussed herein had a period of about one second and lasted for about thirty seconds. The resolution of the Ulysses plasma data, however, was four minutes [*Bame et al.*, 1992], and although high resolution particle measurements are essential for a detailed analysis of shocks and other structures, plasma data could not be included in their analysis.

3. Overview of Paper

This paper is organized as follows: Section 4 gives a cursory overview of reconnection theory. Section 5 addresses the MFI magnetic field data describing the shock, upstream and downstream wave activity, and its propagation direction. Section 6 details the results of a variance analysis applied to the monochromatic wave data. Here we discuss the monochromatic wave polarization and propagation direction. Section 7 introduces Wind/3DP plasma data and shows a clear Doppler shift associated with this monochromatic wave. The Doppler shift allows a determination of the wave plasma frame frequency and the magnitude of the k (wave) vector. Section 8 describes Wind/MASS data which show that associated with this shock was a cold 5 keV proton beam. Section 9 discusses anisotropy information obtained from the MASS instrument. Section 10 shows that the Wind/SWE

instrument observed an electron heat flux drop out associated with the shock indicating a topology change. Section 11 addresses some issues dealing with shock orientation and propagation. Section 12 interprets the observations as resulting from the footpoint of the magnetic cloud reconnecting close to the Sun. Section 13 uses the Wind/MASS observations along with a simple coronal model to place the reconnection site between 1 and 5 solar radii. Finally, Section 14 provides a brief conclusion.

4. Reconnection Theory

Magnetic reconnection, a process believed to operate in and around planetary magnetospheres as well as in the solar corona, releases stored magnetic energy in the form of high velocity streams of ions and electrons and also heats up the particles. Figure 2 shows a simplified diagram of reconnection at an x-type neutral line [*Kivelson and Russell,* 1995]. This process is believed to result from resistivity breaking the frozen-in constraint within a small "dissipation region" (1) which forms around the x-line as shown in Fig. 2. Magnetic field lines and plasma enter the diffusion region from the side (2) and leave from the top and bottom effecting a topology change (3) in which the field lines connect to different partners. Within the diffusion region, the ions are accelerated away from the x-line (4), reaching the Alfvén speed in the outflow region [*Shay et al.,* 1999].

In the Petschek [1964] solution, the acceleration occurs as the plasma passes through slow mode shock waves connected to the diffusion region. This innovation increased the magnetic reconnection rate to realistic levels. A further refinement was made by Sonnerup [1970] who introduced fast mode shocks to loosen the inflow speed constraint on the Petschek model [*Kivelson and Russell,* 1995].

Thus, for the purpose of this work, reconnection carries with it a number of signatures: (i) shocks associated with the reconnection process (ii) topological changes which are frequently deduced by changing particle populations associated with different flux tubes [*Gosling et al.*, 1990]. Here, topological changes are indicated by the presence or absence of field-aligned and anti-field-aligned halo electrons and (iii) ions preferentially accelerated to the Alfvén speed [*Kessel et al.*, 1996].

5. MFI Magnetic Field Data

Figure 3 shows MFI magnetic field data late in hour seventeen of day 292 (October 19) 1995 around the time of the internal shock. The data are high resolution; MFI supplies about eleven magnetic field vectors every second at this time. The shock feature, between hour 17.85118 and 17.85121, makes its transition in less than a tenth of a second. Prior to the transition, in the upstream region, there is pronounced high frequency wave activity, while after the transition, there are low frequency, nearly monochromatic waves which, at first sight, may appear to be an instrumental or analysis-related artifact.

Figure 4 shows the magnetic field magnitude in higher resolution during the time period immediately following the shock transition. The amplitude of the wave starts out at close to one nanotesla, but decays quickly over the course of about thirty seconds. Some residual activity is apparent for at least another thirty seconds after this plot, although at significantly reduced levels. This is common for the Earth's fast mode bow shock due to waves being generated by thermalizing ions in the shock ramp.

Using data from Geotail which observed parts of this magnetic cloud when the bow shock oscillated past the spacecraft, Lepping *et al.* [1997] found a propaga-

tion direction for this internal shock which is within about 20° of the cloud axis. Consequently, it appears that this shock is actually traveling *along* the magnetic cloud, rather than through it, suggestive of a "ducting" mode with the origin at the footpoints of the cloud.

6. Variance Analysis

Figure 5 is a hodogram showing the maximum versus intermediate component of the magnetic field obtained from a variance analysis [*Sonnerup and Cahill,* 1967] performed on the "first" 25 data points (about 2.5 seconds) of the wave. Five data points immediately after the wave rose were eliminated because they "wandered", perhaps because the wave had not completely developed by the time of these five data points. Fig. 5 shows the wave to be elliptically polarized, as one might in general expect.

The minimum variance direction obtained from the variance analysis which we interpret as the propagation direction is

$$\hat{n} = (0.565 , -0.599 , -0.567), \tag{3}$$

where the three components are the GSE x, y, and z directions, respectively, and the field direction is

$$\hat{b} = (0.147 , -0.671 , 0.726), \tag{4}$$

so that $\hat{b} \cdot \hat{n} = 0.073$ ($\theta = 85.8°$) so that the wave appears to be propagating almost perpendicular to the magnetic field (consistent with the bottom two panels of Fig. 3 which show little direction change in the magnetic field), but parallel to the shock normal (within 11°) and parallel to the magnetic cloud axis (within 30°).

The eigenvalue ratios were $\lambda_3/\lambda_1 = 11.7$ and $\lambda_2/\lambda_1 = 2.0$ so that the propagation direction is not well-determined, although the inferred propagation direction fits into our interpretation reasonably well as this propagation direction is consistent with the shock being the source of this monochromatic wave.

Table 1 summarizes the relevant structure angles based on analysis from both this work and Lepping *et al.* [1997]. To a reasonable approximation, the shock normal, magnetic cloud axis, and wave propagation directions are aligned and perpendicular to the magnetic field direction.

Thus, this is a possible electrostatic wave propagating almost perpendicular to the ambient field. Such waves may be important for filling the quasi-linear gap at 90°; that is, they will efficiently scatter particles with large pitch angles [*Karimabadi et al.*, 1992].

7. 3DP Plasma Data

In this study, we use high resolution plasma data from the 3DP instrument [*Lin et al.*, 1995]. Specifically, the most appropriate data set is proton velocity which is obtained at about three second resolution. These solar wind speeds have been compared to the SWE and SMS/MASS data, and, although the time resolution of the latter two instruments is significantly lower than 3DP, the level of agreement is reasonably good, to about 5%. This level of agreement in the absolute value of the solar wind speed provides great confidence in the relative changes in solar wind speed observed by 3DP and used in this study.

Because of the monochromatic nature of this wave, Fourier decomposition was unnecessary. Instead, to determine wave period a simple sine wave was conveniently fit to the magnetic field magnitude and described the data well. Fits were done

during the first 23.1 seconds of magnetic field data following the shock transition when the wave was most evident, prior to being damped out.

Because the intention was to compare the magnetic field wave data with plasma data from the 3DP instrument which yields a measurement every three seconds, three second magnetic field data intervals were selected for fitting to a sine function. The eight panels in Figure 6 show the fits to eight three-second segments of MFI high resolution data. Table 2 lists the fit parameters corresponding to each panel in Fig. 6. Here m_1 is the d.c. offset, m_2 is the amplitude, and m_3 is the frequency. Table 3 compares the fit frequencies to the 3DP velocities at each time. Note the great stability.

Figure 7 shows a plot of the observed wave frequency versus solar wind speed, which, of course, is primarily in the GSE x-direction. The data are reasonably described by a linear relationship with a positive slope, indicating Doppler shifting of the observed frequency with solar wind speed. A fit to the straight line

$$\omega_{obs} = k v_{sw} \cos\theta_{kv_{sw}} - \omega_0, \tag{5}$$

using a value for $\cos\theta_{kv_{sw}}$ of 0.565 from equation (3) allows a determination of the wavelength $\lambda = 2\pi/k$ and the frequency in the solar wind rest frame $\nu_0 = \omega_0/2\pi$. The fit shown in Fig. 7 indicates that $k = 0.19 \pm 0.07$ km^{-1}. This implies a wavelength $\lambda = 33$ km which is relatively close to the shock ramp thickness determined by Lepping *et al.* [1997] of 62 km. The plasma frame frequency $\omega_0 = 39.7 \pm 17.7$ rads/s ($\nu_0 = 6.3$ s^{-1}). As is apparent from an inspection of Fig. 7, there is significant uncertainty on both of these values. These values imply a phase velocity of $\omega_0/k = 209$ km/s.

8. MASS Particle Beam Observations

The high resolution electrostatic mass spectrometer MASS, part of the SMS (SWICS/MASS/STICS) package on the Wind spacecraft, was designed so that the particles pass through a spherical deflection system prior to entering the time-of-flight assembly [*Gloeckler,* 1990; *Gloeckler et al.,* 1995; *Hamilton et al.,* 1990]. Consequently, by using start signal counts, the MASS instrument can function as a standard energy per charge analyzer and can determine solar wind speeds, proton and alpha particle densities and temperatures, and superthermal particle characteristics [*Collier et al.,* 1996; *Collier et al.,* 1998]. Over each spacecraft spin period (about three seconds) the voltage on the deflection plates changes to scan sixty values, so that an entire scan takes about three minutes and covers logarithmically an energy per charge range of 0.52 through 9.89 keV/e with a 4% passband.

During the approximately thirty seconds when the wave intensity was greatest (1751:06-1751:33), the MASS instrument scanned the energy per charge range from about 3.5 to 5.4 keV/e. Figure 8 shows the background adjusted FSR2 (Front Secondary Electron Detection Assembly Rate-2) count rate which is unsectored, that is, contains no directional information.

A statistically significant peak occurs at an energy per charge of about 5 keV/e. If it is assumed that this peak represents a minor ion convecting at the same speed as helium (minor ions tend to convect at the helium speed rather than the proton speed), then the species mass per charge would be about 5.83. This could correspond roughly to iron with charge state +10 (M/Q=56/10=5.6), not an atypical charge state for iron in the solar wind [e.g., *Gloeckler et al.,* 1999]. Although elements and, in particular, iron with unusual charge state distributions have been observed

in magnetic clouds [*Gloeckler,* 1998; *Burlaga et al.,* 1998; *Skoug et al.,* 1999], it is highly unlikely that iron of only this charge state would be enhanced and not the adjacent charge states, +9 and +11. Fig. 8 shows their conspicuous absence (M/Q=56/9=6.22 and 56/11=5.09, as shown on the upper x-axis).

Consequently, we propose that this enhancement is most likely a 5 keV proton beam accelerated by a reconnection process close to the Sun. It is well-known that a two species, three component plasma composed of thermal ions and electrons and an ion beam, is unstable and will lead to wave growth [e.g. *Gary et al.,* 1984]. It is also well-known that upstream of shocks "backstreaming" and "diffuse" ion populations are observed [e.g. *Ipavich et al.,* 1984; *Möbius et al.,* 1986].

The two-paneled Figure 9 shows, as a function of time, the unsectored FSR2 count rate for the 4.91 keV/e bin (top) and the 5.16 keV/e bin (bottom). The highest count rate the 4.91 keV/e channel attained over the entire 28 hour magnetic cloud was during the thirty second monochromatic wave period. Note that (i) the statistical significance of the beam enhancement in the top figure is at the 3σ-4σ level and (ii) the beam is very "narrow". It has a low temperature and a high Mach number, that is the relative width in energy is less than the instrument passband width ($\Delta E/E \leq 0.051$). This determines the lower limit on the velocity over the velocity spread, or the thermal Mach number ($v/\Delta v \geq 2/0.051 = 39.3$).

Finally, these ion observations contain only the energy range scanned by the MASS instrument over the thirty or so seconds during which the wave occurred (spanning 3.46-5.43 keV/e). This is a small fraction of the total energy range MASS scans every three or so minutes (0.52-9.89 keV/e). Consequently, the possibility of other ion beams or interesting features outside the observed 3.46-5.43 keV/e band cannot be ruled out.

Lutsenko and Kudela [1999] have reported more than 200 cases of "almost monoenergetic ions" of very short duration, of the order of one minute, with energies between 30 and 600 keV associated with spacecraft connection to the bow shock. Although we do not believe the monoenergetic beam we observe has a similar physical origin (because the beam we observe is narrower and lower in energy, the wave is only on one side of the shock, and there was no change in the magnetic field direction across the shock), their observations are important because they hint that, contrary to the predictions of the standard shock associated particle models [e.g., *Ipavich et al.,* 1981 and *Lee,* 1982], shocks may produce high energy nearly monochromatic beams.

One possible interpretation of the data involves an ~5 kV shock potential. The higher frequency (upstream) "hashy" waves could then be created by reflected ions off the potential. These reflected ions would in turn create a counter, unstable stream in the solar wind. Also, the energy of this counterstream would be lower (<5 keV), thereby resonating with the higher frequency waves and explaining why the emission appears at higher frequency. The low temperature of the beam may explain the monochromatic nature of the wave. However, the shock potential is generally some fraction of the upstream ion ram kinetic energy [*Mandt and Kan,* 1991], so that 5 kV may be excessively large. Thus, reconnection appears to be the most reasonable explanation for this monoenergetic beam.

9. Monoenergetic Beam Anisotropies

Figure 10 shows, during an hour interval which includes the monochromatic wave period, the *sectored* Front Secondary Electron Detection Assembly rate for the 45 degree sun sector, which observes flow approximately along the negative

GSE x-direction, and for the 315 degree non-sun sector, which is sensitive to particles coming from all other directions. Not surprising, there is a slight background anisotropy ($a_1 \approx 0.089 \pm 0.062$) in approximately the solar wind direction, which may be simply a Compton-Getting effect due to the solar wind flow. However, at the time of the monochromatic wave there is a dramatic increase in the particle anisotropy ($a_1 = 0.363$), indicating a strong anisotropy in the 45° sun sector, centered on the Sun-Earth line.

Particles streaming parallel to the shock normal, which is oriented at about 128° with respect to the GSE x-axis, would all be observed at about 52° off the Sun-Earth line and hence in the 315° MASS non-sun sector. Because these particles are observed primarily in the Sun sector and the magnetic field is primarily in the GSE y-z plane, we conclude that these particles have relatively large pitch angles. However, these anisotropy results are based on only two sectors whose averages could alias fine structure in the angular distributions.

10. SWE Electron Heat Flux Measurements

The presence of energetic electrons greater than about 100 eV or so streaming parallel and/or antiparallel to the magnetic field is generally viewed as a signature of footpoints connected to the Sun, the putative source of the electron heat flux [*Larson et al.,* 1997]. During the course of the magnetic cloud, WIND experienced a variety of different topologies from closed on both ends, to closed on one end, to open on both ends with each open field line region presumably associated with a reconnection event [*Janoo et al.,* 1998; *Crooker et al.,* 1998; *Gosling et al.,* 1995].

Larson *et al.* [1997] interpret the 3DP electron data during this cloud passage as evidence for patchy disconnection of one or both ends of the cloud magnetic field

lines from the Sun. The analysis of Larson *et al.,* [1997] is not alone in suggesting reconnection inside the cloud. Janoo *et al.'s* [1998] results may also be interpreted in this manner.

Figure 11 shows WIND/SWE electron pitch angle distributions during a twenty minute period including the time of the monochromatic wave at four energies, 94 eV, 139 eV, 203 eV, and 298 eV. Prior to the time of the shock, the electrons appear to be streaming antiparallel to the magnetic field indicating connection to the Sun on one end of the magnetic cloud. The shock appears to broaden the pitch angle distribution somewhat, and about nine minutes later, the 180° pitch angle electrons disappear indicating that the topology of the magnetic cloud has transitioned from being connected on one end to being disconnected on both ends, presumably due to a reconnection event. In fact, this may be the strongest argument for reconnection associated with this internal shock. As further evidence supporting this interpretation, the internal shock is moving away from the recently reconnected side of the cloud, as expected if reconnection is the source of the disturbance.

Most observed changes in cloud topology evidenced by the electron pitch angle distributions are interpreted as due to the spacecraft moving between flux tubes with different topologies and are not associated with the magnetic field, plasma, and energetic particle signatures seen around 1750 in the 19 October 1995 cloud. In order to observe these reconnection signatures, the spacecraft must be on the correct field line at whatever time the shock passes. Before the time near shock passage, the field lines will appear connected, and following the time near shock passage, the field lines will appear disconnected. There is a short "window of opportunity," but if this interpretation is correct, eventually other magnetic clouds should be found which show similar shock or shock-like structures.

In fact, a cursory examination of magnetic field data from 34 magnetic clouds observed by Wind between 1995 and 1998 has found three cases, including the October 1995 case discussed here, of shocks internal to magnetic clouds. So, it appears that internal shocks may manifest in about 10% or so of magnetic clouds observed at 1 AU.

In addition, the magnetometer on Ulysses appears to have observed a shock internal to a magnetic cloud at about 5 AU late on day 228 in 1997 [*Forsyth et al.*, 1999] so that this phenomenon is not restricted to 1 AU.

11. Shock Orientation

One of the unusual features of this internal shock is its orientation which is roughly perpendicular to the magnetic field and anti-parallel to the cloud axis (see Table 1). Chao *et al.* [1999] have suggested that the origin of this internal shock is an x-ray flare located at N09W54 on October 16, 1995 at 1221 UT and claim that the interaction of this solar interplanetary disturbance with the magnetic cloud would produce the observed shock orientation.

However, for a number of reasons, we believe reconnection near the footpoints of the CME to be a more natural explanation for the observations as a whole as well as for the shock orientation: (1) The electron observations indicate a topology change which is not predicted by the mechanism proposed by Chao *et al.* (2) The direction of the shock motion is consistent with an origin at the side of the cloud attached to the Sun initially, as deduced from the electron observations (although the direction of shock motion is also consistent with the Chao *et al.* scenario). (3) The energetic ion observations are consistent with reconnection close to the solar surface, which is not predicted by the mechanism proposed by Chao *et al.* (4)

The GOES data for the flare which Chao *et al.* propose as effecting the internal shock is extremely small, barely above background, and may not actually qualify by post-SOHO standards as a "flare". Also, it could be argued that flares are not the best way to look for CMEs which would drive a shock, and that frequently very small flares can have CMEs with them. So, as a further check, SXT data were examined [*Nariaki Nitta,* private communication], but no evidence suggesting a CME was found. Finally, we consulted the Mauna Loa data [*Joan Burkepile,* private communication] for any reports of CMEs. Their white light observations on 16 October 1995 began at about 1726, five hours following the flare at 1221, and it is quite possible that five hours after the flare a CME would be visible in the Mauna Loa field of view. Nevertheless, their observing logs report "no coronal activity" for that day. In summary, although a small flare occurred on 16 October 1995, we have been unable to find any conclusive evidence whatsoever for a CME, let alone a CME driving a shock, which is necessary for the Chao *et al.* mechanism.

Finally, because the main motivation of the proposal of Chao *et al.*, was to explain this internal shock's unusual shock normal direction (56° with the negative GSE x-axis) by postulating an additional interacting shock off the side of the cloud, it should be pointed out that because we expect magnetic clouds to "duct" fast-mode waves, the shock orientation is also consistent with the reconnection interpretation, as stated earlier.

Wave ducting is a well-accepted process for coronal loops close to the Sun [*Ireland,* 1996; *Smith et al.,* 1997]. In the magnetic cloud, the fast mode speed is significantly higher inside the cloud than outside due to its higher magnetic field strength and lower density, so the phase fronts will move quickly within the cloud. Furthermore, the flux rope geometry provides that propagation near the

boundary is frequently quasi-perpendicular to the magnetic field and hence travels faster than the parallel direction [*Hu,* 1998]. Finally, dissipative processes such as viscous dissipation which prevent distrubances from propagating far from their source may be most effective in weak field regions [*Roberts et al.,* 1984; *Gordon and Hollweg,* 1983]. It may be the case that only disturbances in strong field regions (such as in a magnetic cloud) propagate far from their point of origin [*McLean et al.,* 1971].

One can determine whether or not a locomotive is approaching by placing an ear to the railroad tracks. Because sounds travels faster in the metal tracks, the train can be heard in the tracks but not in the air. It is our contention that the magnetic cloud plays the role of the railroad tracks, allowing us to "hear" the remote reconnection event when we would not be able to detect the signatures outside the cloud.

12. Reconnection Model

The reconnection interpretation of these observations is summarized by Figure 12 which illustrates a few field lines (red, black and blue) in the magnetic cloud. According to the electron pitch angle data, Fig. 11, which shows anti-field aligned energetic electron fluxes coming only from one direction, initially one leg of the field is attached to the solar surface while the other has already reconnected. Then, (1) field lines close to the solar surface reconnect and are flung outwards at the local Alfvén speed, about 1000 km/s (the speed of the proton beam observed by MASS), along with the particles on the field lines at the time. This explains the MASS observations of ~5 keV protons associated with the shock–they reflect the Alfvén speed at the reconnection site. This beam may also supply the free energy for the

monochromatic wave. The reconnected field lines initially move much more rapidly than the solar wind, accelerating the solar wind downstream of the disturbance and creating the slight increase in solar wind speed associated with the increase in magnetic field strength. (2) Following the reconnection process, the halo electrons can no longer populate the field lines. (3) The reconnection creates a disturbance in the field lines which propagates mainly within the cloud (because of the reasons cited in Section 11) at the local fast mode speed (the shock velocity in the solar wind frame is 137 km/s and the Alfvén speed is 120 km/s). Thus, the shock observed within the cloud is propagating approximately along the cloud axis (see Table 1). (4) Because the reconnected field lines are thrust outwards at about 1000 km/s, and the field lines in front of them are travelling more slowly, the field after the shock passes maintains the same direction, but is compressed and increases in magnitude as observed in the data shown in Fig. 3. (5) The lack of field-aligned halo electrons suggests that throughout this process the other end of the magnetic cloud was not attached to the Sun.

13. Coronal Model and Reconnection Location

If this reconnection interpretation is correct, then the observed proton beam speed of about 1000 km/s represents approximately the Alfvén speed at the point of reconnection. To determine the range of distances from the solar surface such an Alfvén speed may mark, we examine a simple isothermal hydrostatic two fluid coronal model described by

$$T\frac{\partial \rho}{\partial r} = -\frac{GM_{\odot}m_p}{r^2}\rho + eE, \tag{6}$$

for the protons and

$$T\frac{\partial \rho}{\partial r} = -eE, \tag{7}$$

for the electrons. Here, T is the temperature, ρ is the density, G is the universal gravitational constant, $M_\odot$ is the solar mass, m_p is the proton mass, and r is the distance from the Sun. Although taking the electron and proton temperatures to be identical constitutes a bad assumption in the solar wind, for the purposes of determining the Alfvén speed it is not critical because the mass density is determined by the protons and the scale height by the average of the proton and electron temperatures.

Subtracting the two equations allows a determination of the electric field

$$E = \frac{GM_\odot m_p}{2r^2 e}\rho. \tag{8}$$

Plugging this back into the ion equation (4) and solving for the density yields

$$\rho(r) = \rho_0 \exp\left\{-\frac{1.15\text{x}10^7}{T|_K}\left(1 - \frac{r_0}{r}\right)\right\}, \tag{9}$$

where $T|_K$ is the temperature in Kelvin. If the expansion is assumed radial and flux is conserved, then the magnetic field magnitude may be determined by

$$B(r) = B_0\left(\frac{r_0}{r}\right)^2, \tag{10}$$

and the Alfvén speed, v_A, using the relation

$$v_A = \frac{B}{\sqrt{\mu_0 \rho}} = 892\frac{B}{\sqrt{\rho}}, \tag{11}$$

where B is in Tesla, ρ is in kg/m^3 and v_A is in m/s.

Using this model with a reasonable range of values for T, ρ_0 and B_0 at one solar radii produces an Alfvén speed of about 1000 km/s (the speed of the proton beam observed by MASS) at a distance of between 1 and 5 or so solar radii. Figure 13 shows the model results for Alfvén speed and density for T = 1.6x10^6 K, ρ_0 =

$1.7\text{x}10^{-12}$ kg/m^3, and $B_0 = 1.3\text{x}10^{-3}$ T. The $1.3\text{x}10^{-3}$ T magnetic field value represents a radial extrapolation of the observed 28 nT Wind field back to the solar surface. As the field probably expands superradially, this likely underestimates the field somewhat. Also, because the slow (i.e. equatorial) solar wind flow is believed to be subsonic to about four solar radii, the inclusion of solar wind flow will not affect the model Alfvén speed significantly in the region of interest. These radial distances for reconnection are reasonable and support the scenario that WIND is observing reconnection remnants inside the October 18-19, 1995 magnetic cloud.

14. Conclusion

We have presented WIND observations from MFI, 3DP, SMS, and SWE inside the October 18-20, 1995 magnetic cloud which may be interpreted as evidence of reconnection occurring at low altitudes in the solar corona, between 1 and 5 solar radii. The observations include an internal shock travelling approximately along the axis of the magnetic cloud, simple compression of the magnetic field consistent with the footprint magnetic fields being thrust outwards at speeds much greater than the solar wind speed, an electron heat flux drop out occurring within minutes of the shock indicating a topological change resulting from disconnection from the solar surface and a very cold 5 keV proton beam resulting from reconnection. In addition, an unusually monochromatic wave propagating perpendicular to the magnetic field was observed in association with the shock and may be related to the monoenergetic particle beam.

Because the spacecraft must be fortuitously positioned to observe the shock when it passes, observations such as the ones reported here will be rare. Furthermore, because shocks will expand, it may be possible to observe a shock internal

to a magnetic cloud without a corresponding topology change or energetic particle beam. However, if our interpretation is correct, given observations of enough magnetic clouds with sophisticated instrumentation, similar observations inside magnetic clouds should surface in the future, particularly as we transition to solar maximum and magnetic clouds become more frequent. Consistent with this, a few magnetic clouds have been found to possess internal shocks.

Acknowledgments. This research was performed in part while Michael R. Collier was a National Research Council Resident Research Associate in the Electrodynamics Branch, Code 696, at the NASA/Goddard Space Flight Center. Thanks to Larry Bleau at the University of Maryland for helping us access MASS data. Also thanks to Joan Burkepile and Nariaki Nitta for helping us get data and images.

References

Bame, S.J., D.J. McComas, B.L. Barraclough, J.L. Phillips, K.J. Sofaly, J.C. Chavez, B.E. Goldstein, and R.K. Sakurai, The Ulysses solar wind plasma experiment, *Astron. Astrophys. Suppl. Ser., 92*, 237-265, 1992.

Burlaga, L., E. Sittler, F. Mariani, and R. Schwenn, Magnetic loop behind an interplanetary shock: Voyager, Helios, and IMP 8 observations, *J. Geophys. Res., 86*, 6673-6684, 1981.

Burlaga, L.F., Interplanetary Magnetohydrodynamics, Oxford University Press, New York, pp. 89-114, 1995.

Burlaga, L., R. Fitzenreiter, R. Lepping, K. Ogilvie, A. Szabo, A. Lazarus, J. Steinberg, G. Gloeckler, R. Howard, D. Michels, C. Farrugia, R.P. Lin, and D.E. Larson, A magnetic cloud containing prominence material: January 1997, *J. Geophys. Res., 103*, 277-285, 1998.

Chao, J.K., C.B. Wang, D.J. Wu, and R.P. Lepping, Interaction of the Oct. 14-19, 1995 magnetic cloud with a solar interplanetary disturbance, *EOS, Transactions, American Geophysical Union, 1999 Spring Meeting (Supplement), 80,* SH51C-06, S269, 1999.

Christon, S.P., C.S. Cohen, G. Gloeckler, T.E. Eastman, A.B. Galvin, F.M. Ipavich, Y.-K. Ko, A.T.Y. Lui, R.A. Lundgren, R.W. McEntire, E.C. Roelof, and D.J. Williams, Concurrent observations of solar wind oxygen by Geotail in the magnetosphere and Wind in interplanetary space, *Geophys. Res. Lett., 25*, 2987-2990, 1998.

Collier, Michael R.. D.C. Hamilton, G. Gloeckler, P. Bochsler, and R.B. Sheldon, Neon-20, oxygen-16, and helium-4 densities, temperatures, and superthermal tails in the solar wind determined with WIND/MASS, *Geophys. Res. Lett.,*

23, 1191-1194. 1996.

Collier, Michael R., D.C. Hamilton, G. Gloeckler, G. Ho, P. Bochsler, R. Bodmer, and R. Sheldon, Oxygen 16 to oxygen 18 abundance ratio in the solar wind observed by Wind/MASS, *J. Geophys. Res., 103*, 7-13, 1998.

Crooker, N.U., A.H. McAllister, R.J. Fitzenreiter, J.A. Linker, D.E. Larson, R.P. Lepping, A. Szabo, J.T. Steinberg, A.J. Lazarus, Z. Mikic, and R.P. Lin, Sector boundary transformation by an open magnetic cloud, *J. Geophys. Res., 103*, 26,859-26,868, 1998.

Forsyth, R.J., A. Balogh, E.J. Smith, and J.T. Gosling, Magnetic field structure of transients at Ulysses: Their relationship to coronal structure and CMEs, IUGG 99 Birmingham, Abstracts, GA4.01/W/13-A2, p. A.361, 1999.

Fox, N.J., M. Peredo, and B.J. Thompson, Cradle to grave tracking of the January 6-11, 1997 Sun-Earth connection event, *Geophys. Res. Lett., 25*, 2461-2464, 1998.

Gary, S. Peter, Charles W. Smith, Martin A. Lee, Melvyn L. Goldstein, and David W. Fooslund, Electromagnetic ion beam instabilities, *Phys. Fluids, 27*, 1852-1862, 1984.

Gloeckler, G., Ion composition measurement techniques for space plasmas, *Rev. Sci. Instrum., 61*, 3613-3620, 1990.

Gloeckler, G., Solar wind composition measurements from the SWICS and SWIMS instrument on ACE, *EOS, Transactions, American Geophysical Union, 1998 Spring Meeting (supplement), 79*, S259, 1998.

Gloeckler, G., H. Balsiger, A. Bürgi, P. Bochsler, L.A. Fisk, A.B. Galvin, J. Geiss, F. Gliem, D.C. Hamilton, T.E. Holzer, D. Hovestadt, F.M. Ipavich, E. Kirsch, R.A. Lundgren. K.W. Ogilvie, R.B. Sheldon, and B. Wilken, The solar wind

and suprathermal ion composition investigation on the Wind spacecraft, *Space Sci. Rev., 71*, 79-124, 1995.

Gloeckler, G., L.A. Fisk, S. Hefti, N.A. Schwadron, T.H. Zurbuchen, F.M. Ipavich, J. Geiss, P. Bochsler and R.F. Wimmer-Schweingruber, Unusual composition of the solar wind in the 2-3 May 1998 CME observed with SWICS on ACE, *Geophys. Res. Lett., 26*, 157-160, 1999.

Gordon, B.E. and J.V. Hollweg, Collisional damping of surface waves in the solar corona, *Astrophys. J., 266*, 373-382, 1983.

Gosling, J.T., Coronal mass ejections and magnetic flux ropes in interplanetary space, in "Physics of Magnetic Flux Ropes," C.T. Russell, E.R. Priest and L.C. Lee (eds.), *Geophys. Mono. 58*, Amer. Geophys. Union, 343-364, 1990.

Gosling, J.T., M.F. Thomsen, S.J. Bame, T.G. Onsager and C.T. Russell, The electron edge of the low latitude boundary layer during accelerated flow events, *Geophys. Res. Lett., 17*, 1833-1836, 1990.

Gosling, J.T., J. Birn, and M. Hesse, Three-dimensional magnetic reconnection and the magnetic topology of coronal mass ejection events, *Geophys. Res. Lett., 22*, 869-872. 1995.

Hamilton, D.C., G. Gloeckler, F.M. Ipavich, R.A. Lundgren, R.B. Sheldon, and D. Hovestadt, New high-resolution electrostatic ion mass analyzer using time of flight, *Rev. Sci. Instrum., 61*, 3104-3106, 1990.

Hu, Y.Q., Asymmetric propagation of flare-generated shocks in the heliospheric equatorial plane, *J. Geophys. Res., 103*, 14,631-14,641, 1998.

Ipavich, F.M., A.B. Galvin, G. Gloeckler, M. Scholer and D. Hovestadt, A statistical survey of ions observed upstream of the Earth's bow shock: Energy spectra, composition. and spatial variation, *J. Geophys. Res., 86*, 4337-4342, 1981.

Ipavich, F.M., J.T. Gosling, and M. Scholer, Correlation between the He/H ratios in upstream particle events in the solar wind, *J. Geophys. Res., 89*, 1501-1507, 1984.

Ireland, J., Wave heating of the solar corona and SoHO, *Ann. Geophysicae, 14*, 485-491, 1996.

Janoo, L., C.J. Farrugia, R.B. Torbert, J.M. Quinn, A. Sazbo, R.P. Lepping, K.W. Ogilvie, R.P. Lin, D. Larson, J.D. Scudder, V.A. Osherovich, and J.T. Steinberg, Field and flow perturbations in the October 18-19, 1995, magnetic cloud, *J. Geophys. Res., 103*, 17,249-17,259, 1998.

Karimabadi, H., D. Krauss-Varban, and T. Terasawa, Physics of pitch angle scattering and velocity diffusion 1. Theory, *J. Geophys. Res., 97*, 13,853-13,864, 1992.

Kessel, R.L., S.-H. Chen, J.L. Green, S.F. Fung, S.A. Boardsen, L.C. Tan, T.E. Eastman, J.D. Craven, and L.A. Frank, Evidence of high-latitude reconnecting during nothward IMF: Hawkeye observations, *Geophys. Res. Lett., 23*, 583-586, 1996.

Kivelson, M.G. and C.T. Russell, Introduction to Space Physics, Cambridge University Press, Cambridge, pp. 236-284, 1995.

Laakso, H., D.H. Fairfield, M.R. Collier, H. Opgenoorth, T.-D. Phan, D.G. Sibeck, B.L. Giles, H.J. Singer, R.P. Lepping, R.P. Lin, F.S. Mozer, R.F. Pfaff, K. Tsuruda, and J.R. Wygant, Oscillations of magnetospheric boundaries driven by IMF rotations, *Geophys. Res. Lett., 25*, 3007-3010, 1998.

Larson, D.E., R.P. Lin, J.M. McTiernan, J.P. McFadden, R.E. Ergun, M. McCarthy, H. Rème, T.R. Sanderson, M. Kaiser, R.P. Lepping, and J. Mazur, Tracing the topology of the October 18-20, 1995, magnetic cloud with $\sim$0.1-10^2 keV

electrons, *Geophys. Res. Lett., 24*, 1911-1914, 1997.

Lee, M.A., Coupled hydromagnetic wave excitation and ion acceleration upstream of the Earth's bow shock, *J. Geophys. Res., 87*, 5063-5080, 1982.

Lepping, R.P., M.H. Acuña, L.F. Burlaga, W.M. Farrell, J.A. Slavin, K.H. Schatten, F. Mariani, N.F. Ness, F.M. Neubauer, Y.C. Whang, J.B. Byrnes, R.S. Kennon, P.V. Panetta, J. Scheifele, and E.M. Worley, The WIND magnetic field investigation, *Space Sci. Rev., 71*, 207-229, 1995.

Lepping, R.P., L.F. Burlaga, A. Szabo, K.W. Ogilvie, W.H. Mish, D. Vassiliadis, A.J. Lazarus, J.T. Steinberg, C.J. Farrugia, L. Janoo, and F. Mariani, The Wind magnetic cloud and events of October 18-20, 1995: Interplanetary properties and as triggers for geomagnetic activity, *J. Geophys. Res., 102*, 14,049-14,063, 1997.

Low, B.C. and J.R. Hundhausen, Magnetostatic structures of the solar corona II. The magnetic topology of quiescent prominences, *Ap. J., 443*, 818-836, 1995.

Lin, R.P., K.A. Anderson, S. Ashford, C. Carlson, D. Curtis, R. Ergun, D. Larson, J. McFadden, M. McCarthy, G.K. Parks, H. Rème, J.M. Bosqued, J. Coutelier, F. Cotin, C. D'Uston, K.-P. Wenzel, T.R. Sanderson, J. Henrion, J.C. Ronnet, and G. Paschmann, A three-dimensional plasma and energetic particle investigation for the Wind spacecraft, *Space Sci. Rev., 71*, 125-153, 1995.

Lucek, E.A. and A. Balogh, Ulysses observations of a discrete wave packet upstream of an interplanetary shock, *Geophys. Res. Lett., 24*, 2387-2390, 1997.

Lutsenko and Kudela, Almost monoenergetic ions near the Earth's magnetosphere boundaries, *Geophys. Res. Lett., 26*, 413-416, 1999.

Mandt, M.E. and J.R. Kan, Electrostatic potential jump across fast-mode collision-

less shocks, *J. Geophys. Res., 96*, 21,391-21,395, 1991.

McLean, D.J., K.V. Sheridan, R.T. Stewart and J.P. Wild, Regular pulses from the Sun and a possible clue to the origin of solar cosmic rays, *Nature, 234*, 140-142, 1971.

Moore, T.E., W.K. Peterson, C.T. Russell, M.O. Chandler, M.R. Collier, H.L. Collin, P.D. Craven, R. Fitzenreiter, B.L. Giles, and C.J. Pollock, Ionospheric mass ejection in response to a CME, *Geophys. Res. Lett., 26*, 2339-2342, 1999.

Möbius, E., D. Hovestadt, B. Klecker, M. Scholer, F.M. Ipavich, C.W. Carlson, and R.P. Lin, A burst of energetic O+ ions during an upstream particle event, *Geophys. Res. Lett., 13*, 1372, 1986.

Ogilvie, K.W., D.J. Chornay, R.J. Fitzenreiter, F. Hunsaker, J. Keller, J. Lobell, G. Miller, J.D. Scudder, E.C. Sittler, Jr., R.B. Torbert, D. Bodet, G. Needell, A.J. Lazarus, J.T. Steinberg, J.H. Tappan, A. Mavretic and E. Gergin, SWE, A comprehensive plasma instrument for the Wind spacecraft, *Space Sci. Rev., 71*, 55-77, 1995.

Osherovich, V.A., C.J. Farrugia, and L.F. Burlaga, Dynamics of aging magnetic clouds, *Adv. Space Res.*, **13.6**(6), 57-62, 1993.

Osherovich, Vladimir A., J. Fainberg, and R.G. Stone, Multi-tube model for interplanetary magnetic clouds, *Geophys. Res. Lett. 26,* 401-404, 1999.

Petschek, H.E., Magnetic field annihilation, in AAS-NASA Symposium on The Physics of Solar Flares (ed. W.N. Hess), NASA SP-50, Washington, D.C., pp. 425-439, 1964.

Priest, E.R., Solar Magnetohydrodynamics, D. Reidel Publishing Company, Dordrecht, Holland, p. 125, 1987.

Roberts, B., P.M. Edwin, and A.O. Benz, On coronal oscillations, *Astrophys. J.*,

279, 857-865, 1984.

Shay, M.A., J.F. Drake, B.N. Rogers, and R.E. Denton, The scaling of collisionless, magnetic reconnection for large systems, *Geophys. Res. Lett., 26*, 2163-2166, 1999.

Skoug, R.M., S.J. Bame, W.C. Feldman, J.T. Gosling, D.J. McComas, J.T. Steinberg, R.L. Tokar, P. Riley, L.F. Burlaga, N.F. Ness, and C.W. Smith, A prolonged He^+ enhancement within a coronal mass ejection in the solar wind, *Geophys. Res. Lett., 26*, 161-164, 1999.

Smith, J.M., B. Roberts, and R. Oliver, Ducted fast waves in coronal loops: curvature effects, *Astron. Astrophys., 317*, 752-760, 1997.

Sonnerup, B. U. Ö., Magnetic-field re-connexion in a highly conducting incompressible fluid, *J. Plasma Phys., 4*, 161-174, 1970.

Sonnerup, B. U. Ö. and L.J. Cahill, Jr., Magnetopause structure and attitude from *Explorer* 12 observations, *J. Geophys. Res., 72*, 171-183, 1967.

Takeuchi, T., T. Araki, R.P. Lepping, T. Yamamoto, S. Kokubun, T. Nagai, and T. Iyemori, A magnetic cloud with unusual structure and corresponding bow shock movement observed on May 13, 1995, *Geophys. Res. Lett., 25*, 3269-3272, 1998.

Wu, S.T., W.P. Guo, and J.F. Wang, Dynamical evolution of a coronal streamer-bubble system 1. A self-consistent planar magnetohydrodynamic simulation, *Solar Physics, 157*, 325-348, 1995.

Figure Captions

Figure 1. Overview of the Wind MFI and SWE magnetic field and plasma observations during the October 18-19, 1995 magnetic cloud. The interior of the cloud is marked with the two-headed arrow, although there is some ambiguity about the back of the cloud. The internal shock is most evident in the magnetic field magnitude, in the first panel, whereas the magnetic field direction, given in the second and third panels, varies little across the shock. The density, thermal speed and velocity all increase across this shock so that it shows characteristics of a fast forward MHD shock. The shock speed is very close to the Alfvén speed, approximately the fast-mode speed.

Figure 2. Reconnection process at an x-type neutral line. Magnetic field and plasma are accelerated in the diffusion region (1) after entering from the left and right (2). The field lines and plasma are ejected towards the top and bottom effecting a topology change (3). The ions are preferentially accelerated to the Alfvén speed (4).

Figure 3. Overview of the MFI high resolution (eleven vectors every second) magnetic field data showing the "shock" inside the October 18-20 magnetic cloud. The top panel shows the magnetic field magnitude in nanotesla with the second through fourth panels showing the individual GSE components of the magnetic field. The fifth and sixth panels show the θ (out of the ecliptic) and ϕ (in the ecliptic) angles of the magnetic field. The shock transition occurs between hour 17.85118 and 17.85121 on day 292 (October 19) with the monochromatic wave immediately following and lasting about thirty seconds. There are hashy high frequency waves ($\gg$1 Hz) present on the upstream side. Note that the magnetic field angle changes

very little during this time period.

Figure 4. The magnetic field magnitude during about thirty seconds immediately following the shock transition. The monochromatic wave activity is most pronounced but decaying in amplitude during this thirty second interval, although some trace of the activity, at a much lower level, is present for a minute or so after the shock transition.

Figure 5. Hodogram showing maximum versus intermediate component for the "first" 25 data points of the wave. The eigenvalue ratios of the variance analysis are $\lambda_{int}/\lambda_{min} = 2.0$ and $\lambda_{max}/\lambda_{int} = 5.7$ so that the propagation direction is not exceptionally well-determined. Note that the wave appears to be elliptically polarized.

Figure 6. These eight panels show the sine fits to three second intervals of MFI high resolution magnetic field magnitude data. The shock jump occurs at hour 17.85121 with a wave significantly damped by about hour 17.8593. The wave duration was 23.1 seconds and the functional form fit was $m_1+m_2\cdot\cos(3600\cdot m_3\cdot(m_0-\text{start time}))$ where "start time" is the beginning of the three second data interval. Phase was eliminated by starting and ending on a complete half cycle. The values for m_1, m_2, and m_3, as well as the start time used for each panel (a-h) are listed in Table 2.

Figure 7. The observed frequencies in the Wind spacecraft frame obtained from the fits shown in Fig. 6 plotted versus the observed 3DP three-second solar wind speed data. If the Doppler shifting is assumed to obey $\omega_{obs} = kv_{sw}\cos\theta_{kv_{sw}} + \omega_0$ where k is the wave vector and ω_0 is the rest frame wave frequency, then the fit given by the solid line provides $\omega_0 = -39.7 \pm 17.7$ radians/s and $k = 0.19 \pm 0.07$ km^{-1}. The correlation coefficient for these data is 0.73.

Figure 8. The background adjusted SMS/MASS FSR2 count rate during the wave time period (17 5106-5133). The time periods used for background subtraction were 17 4500-4528 and 17 5409-5437, which cover the same energy per charge range. A clear, statistically significant peak occurs at an energy per charge of about five keV/e. The mass per charge (indicated at the top of the plot) corresponding to iron of charge state +10 is indicated by the arrow, although it is argued the beam is probably suprathermal protons.

Figure 9. Counts in the 4.91 keV/e and 5.16 keV/e energy per charge bins as a function of time over a one hour interval from 17:20-18:20. The beam is very "narrow" in velocity space.

Figure 10. The sectored FSR rate for both the 45° sun and the 135° non-sun sectors for the energy per charge bin 4.91 keV/e are plotted on the left and right y-axes, respectively. The logarithmic y-axes are offset by a factor of seven to account for the disparate angular ranges of the two sectors.

Figure 11. WIND/SWE electron pitch angle distributions around the time of the internal shock-like feature. The four panels show four energies: 94 eV, 139 eV, 203 eV, and 298 eV. Prior to the shock, the electrons appear to be primarily streaming at 180° pitch angle. The shock appears to broaden the pitch angle distribution, and about nine minutes after the shock, the streaming electrons disappear.

Figure 12. Schematic summary of the reconnection interpretation for the WIND observations inside the magnetic cloud of October 18-19, 1995. Initially, a field line disconnects from the solar surface and is flung outwards at ~1000 km/s. The reconnection event triggers a disturbance in the field lines which propagates along the cloud axis. The field lines before and after the discontinuity maintain their

direction, but are compressed.

Figure 13. Sample results for the Alfvén speed and the density as a function of distance from the solar surface for a simple isothermal hydrostatic two fluid coronal model using a coronal temperature of 1.6×10^6 Kelvin, a density of 1.7×10^{-12} kg/m^3, and a magnetic field of 1.3×10^{-3} Tesla. This model is used to place the location of the reconnection point between 1 and 5 solar radii. The one solar radius field value used represents a radial extrapolation of the 28 nT field observed at Wind back to the Sun and as such represents a lower bound for the field at the Sun since most probably the field expands superradially.

Matrix of Angles

	cloud axis	shock normal	wave propagation
shock normal	159° (∥)	—	—
wave propagation	31° (∥)	169° (∥)	—
magnetic field	59° (⊥)	105° (⊥)	86° (⊥)

Table 1

panel	m_1 (nT)	m_2 (nT)	m_3 (rads/s)	start time (hr)
a	27.99	0.66	6.03	17.85218
b	27.80	0.75	6.10	17.85308
c	27.73	-0.63	5.98	17.85384
d	27.71	-0.49	6.37	17.85471
e	27.68	-0.62	6.46	17.85558
f	27.65	0.49	6.24	17.85647
g	27.62	0.46	6.41	17.85732
h	27.65	0.25	6.61	17.85816

Table 2

time (hour)	MFI ω_0 (rads/s)	3DP $\|\mathbf{v}\|$ (km/s)
17.85256	6.03 ± 0.03	424.28
17.85341	6.10 ± 0.05	421.83
17.85426	5.98 ± 0.05	424.02
17.85510	6.37 ± 0.03	425.93
17.85595	6.46 ± 0.04	426.32
17.85680	6.24 ± 0.04	424.31
17.85765	6.41 ± 0.05	424.31
17.85850	6.61 ± 0.06	426.32

Table 3

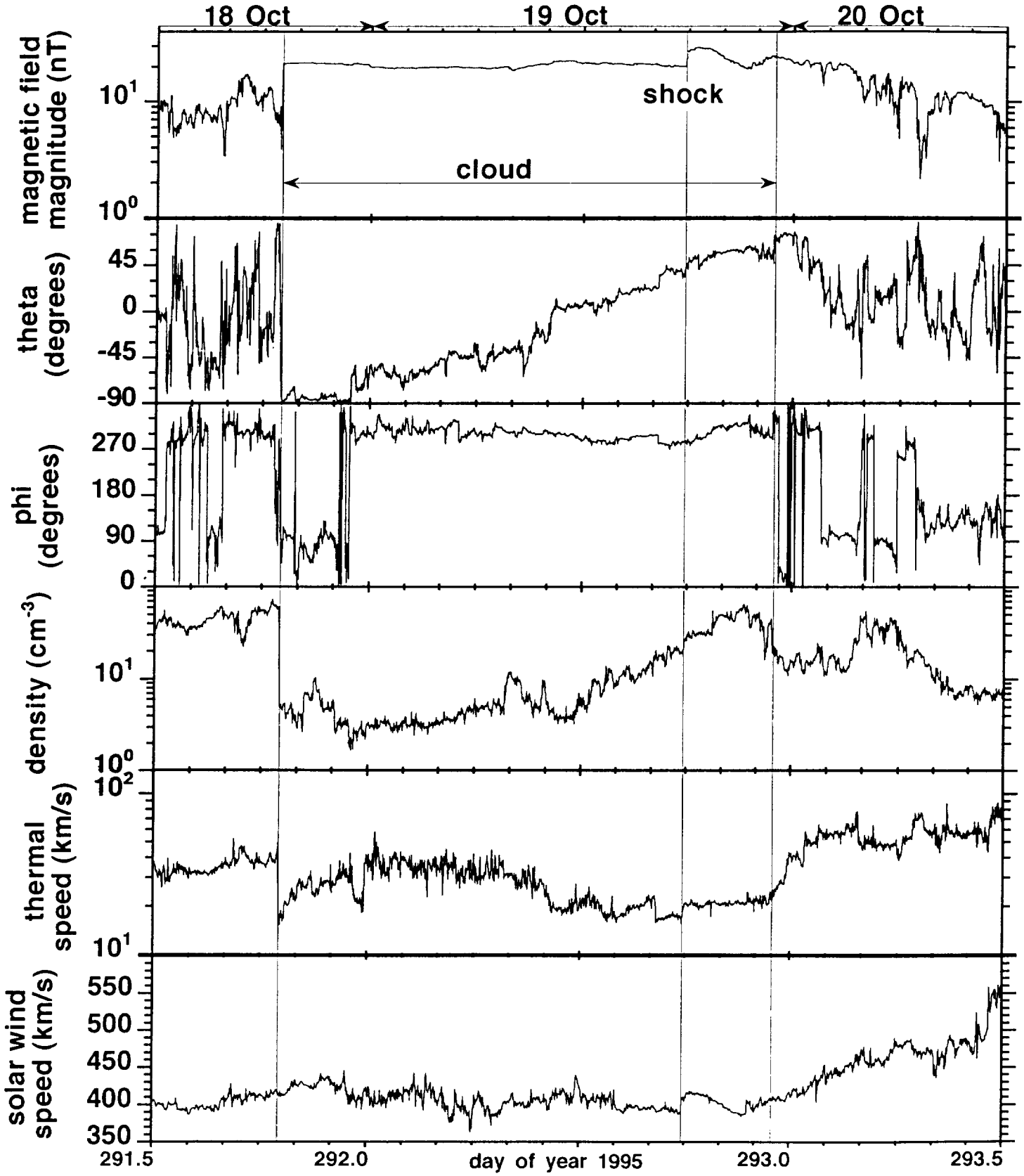
18 Oct
19 Oct
20 Oct
magnetic field magnitude (nT)
10^1
10^0
shock
cloud
theta (degrees)
45
0
-45
-90
phi (degrees)
270
180
90
0
density (cm^{-3})
10^1
10^0
thermal speed (km/s)
10^2
10^1
solar wind speed (km/s)
550
500
450
400
350
291.5
292.0
day of year 1995
293.0
293.5

Figure 1

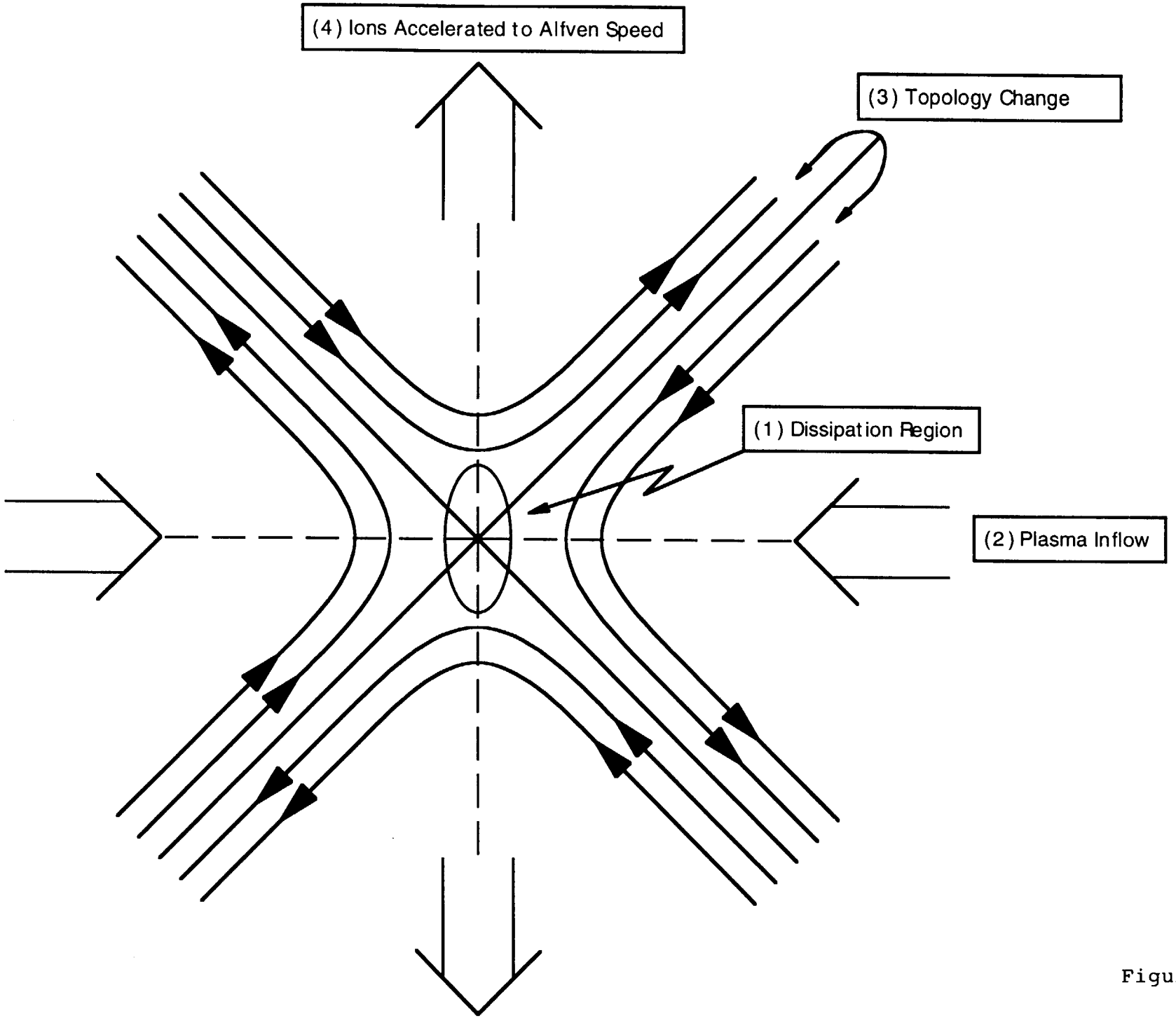
(4) Ions Accelerated to Alfven Speed
(3) Topology Change
(1) Dissipation Region
(2) Plasma Inflow

Figure 2

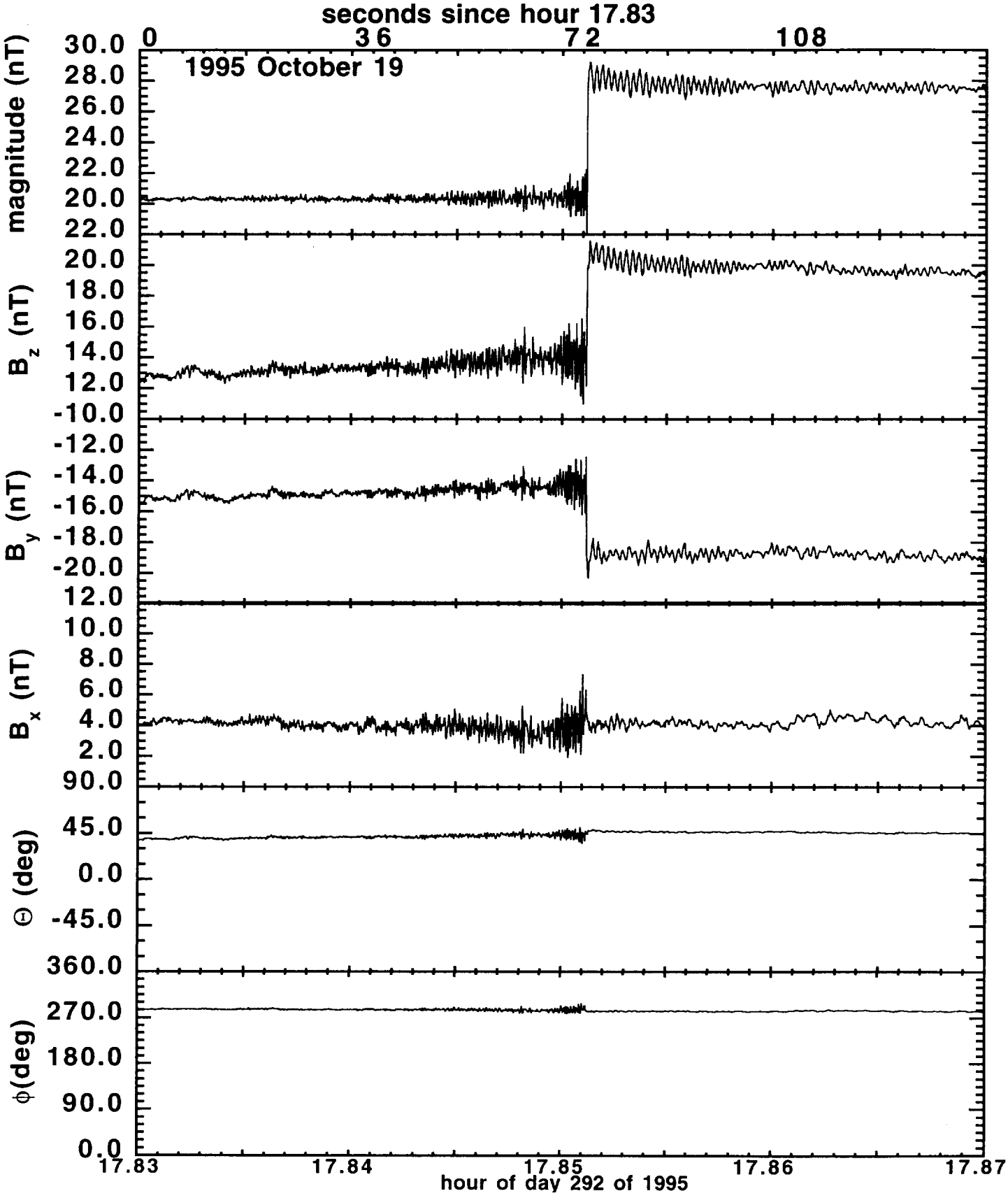
seconds since hour 17.83
0
36
72
108
1995 October 19
magnitude (nT)
30.0
28.0
26.0
24.0
22.0
20.0
B_z (nT)
20.0
18.0
16.0
14.0
12.0
-10.0
B_y (nT)
-12.0
-14.0
-16.0
-18.0
-20.0
12.0
B_x (nT)
10.0
8.0
6.0
4.0
2.0
90.0
Θ (deg)
45.0
0.0
-45.0
360.0
ϕ(deg)
270.0
180.0
90.0
0.0
17.83
17.84
17.85
17.86
17.87
hour of day 292 of 1995

Figure 3

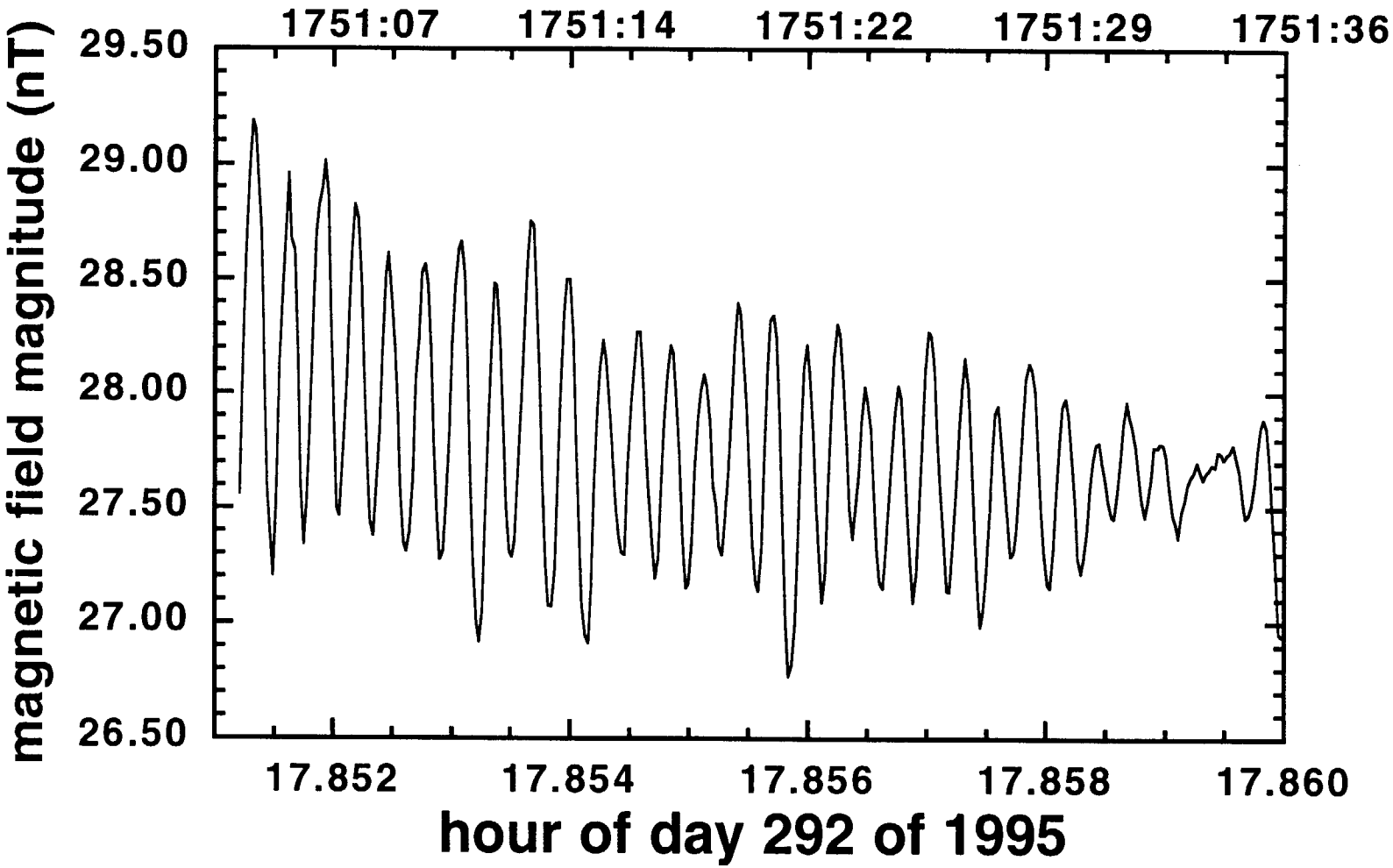
1751:07
1751:14
1751:22
1751:29
1751:36
29.50
29.00
28.50
28.00
27.50
27.00
26.50
magnetic field magnitude (nT)
17.852
17.854
17.856
17.858
17.860
hour of day 292 of 1995

Figure 4

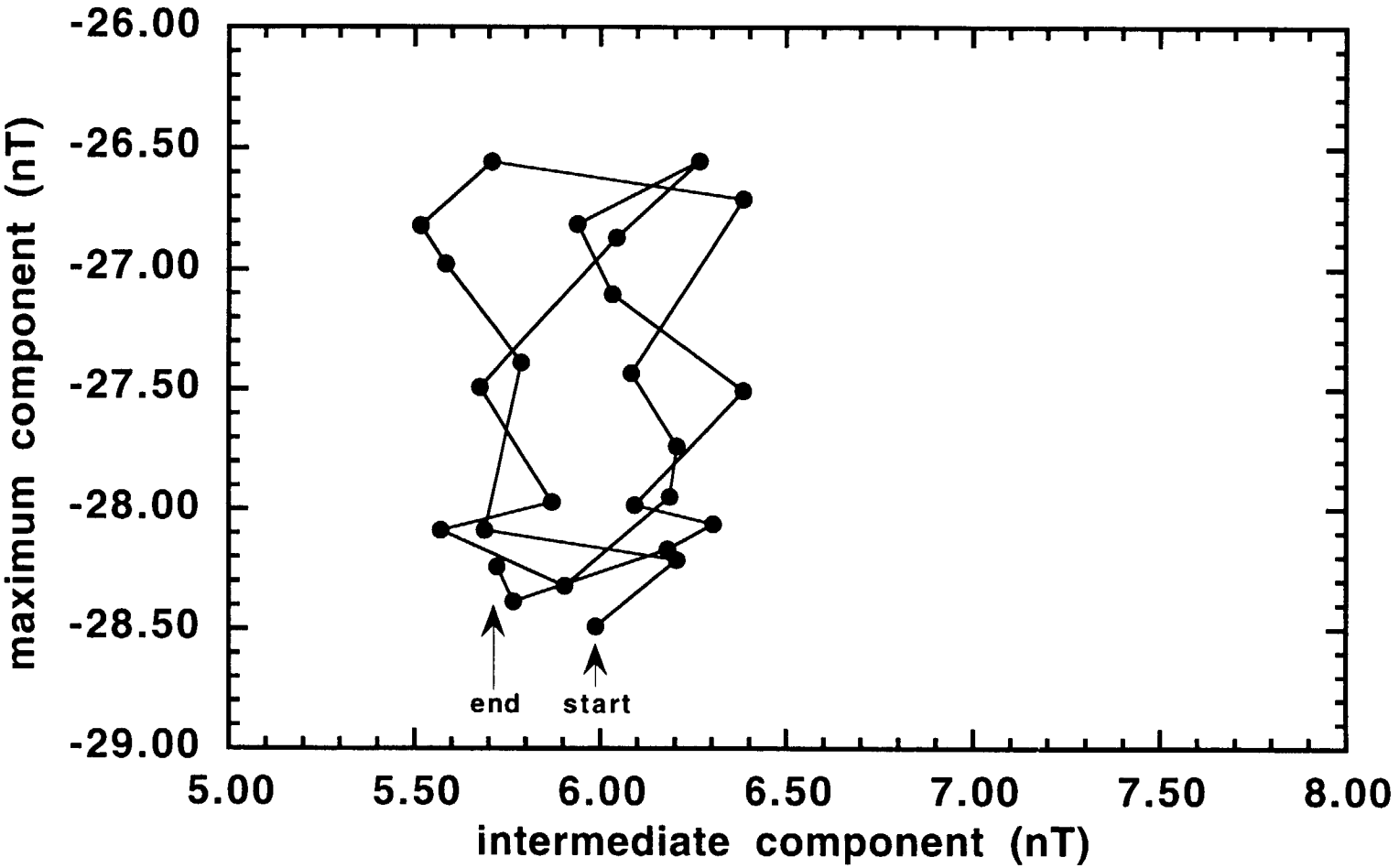
-26.00
-26.50
-27.00
-27.50
-28.00
-28.50
-29.00
maximum component (nT)
end
start
5.00
5.50
6.00
6.50
7.00
7.50
8.00
intermediate component (nT)

Figure 5

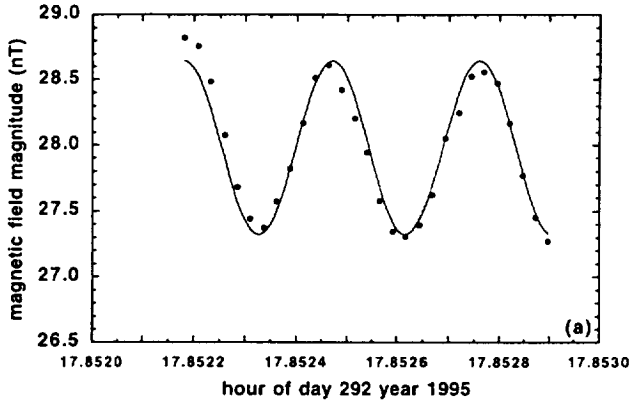
magnetic field magnitude (nT)
29.0
28.5
28.0
27.5
27.0
26.5
17.8520
17.8522
17.8524
17.8526
17.8528
17.8530
hour of day 292 year 1995
(a)

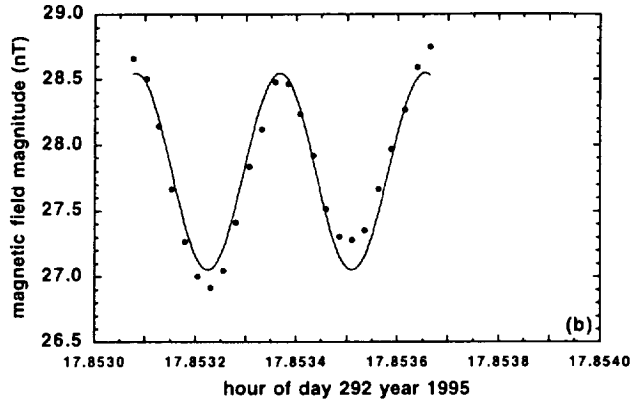
magnetic field magnitude (nT)
29.0
28.5
28.0
27.5
27.0
26.5
17.8530
17.8532
17.8534
17.8536
17.8538
17.8540
hour of day 292 year 1995
(b)

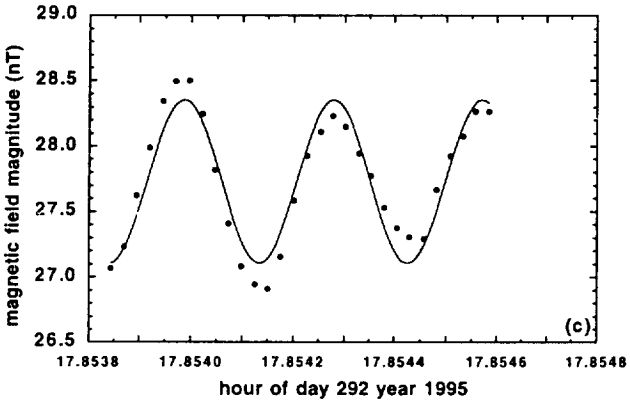
magnetic field magnitude (nT)
29.0
28.5
28.0
27.5
27.0
26.5
17.8538
17.8540
17.8542
17.8544
17.8546
17.8548
hour of day 292 year 1995
(c)

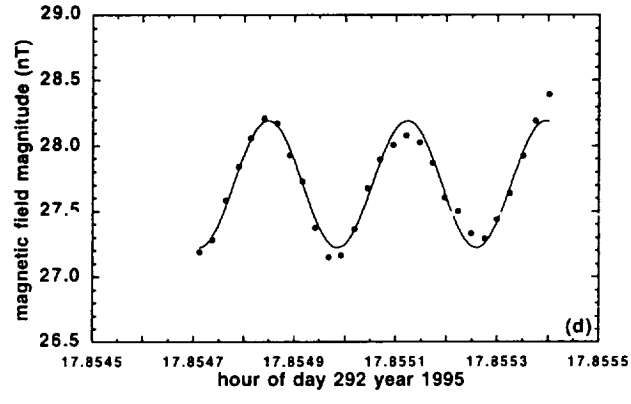
magnetic field magnitude (nT)
29.0
28.5
28.0
27.5
27.0
26.5
17.8545
17.8547
17.8549
17.8551
17.8553
17.8555
hour of day 292 year 1995
(d)

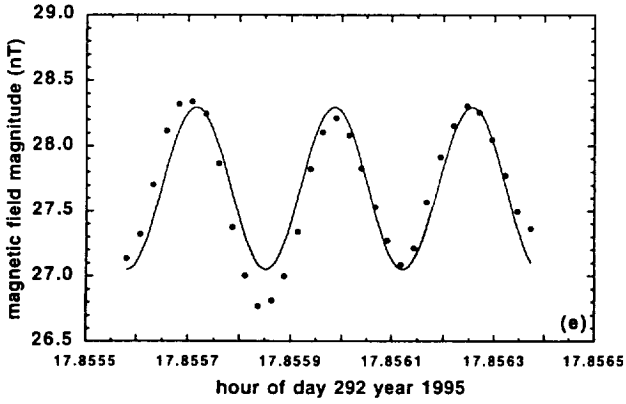
magnetic field magnitude (nT)
29.0
28.5
28.0
27.5
27.0
26.5
17.8555
17.8557
17.8559
17.8561
17.8563
17.8565
hour of day 292 year 1995
(e)

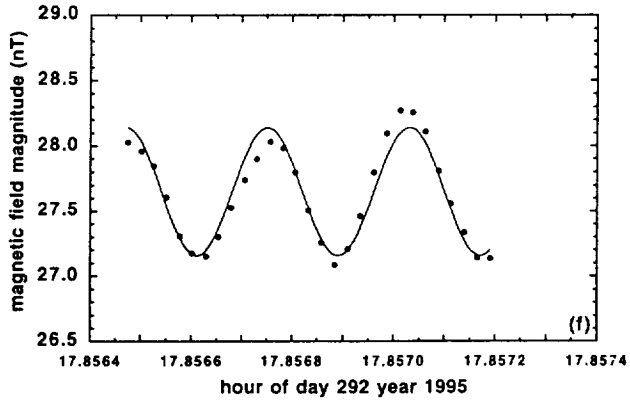
magnetic field magnitude (nT)
29.0
28.5
28.0
27.5
27.0
26.5
17.8564
17.8566
17.8568
17.8570
17.8572
17.8574
hour of day 292 year 1995
(f)

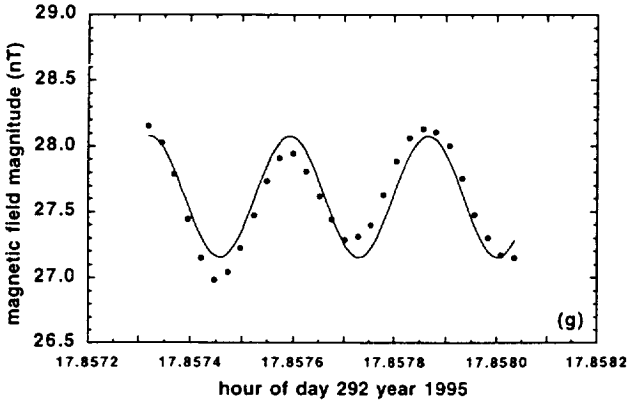
magnetic field magnitude (nT)
29.0
28.5
28.0
27.5
27.0
26.5
17.8572
17.8574
17.8576
17.8578
17.8580
17.8582
hour of day 292 year 1995
(g)

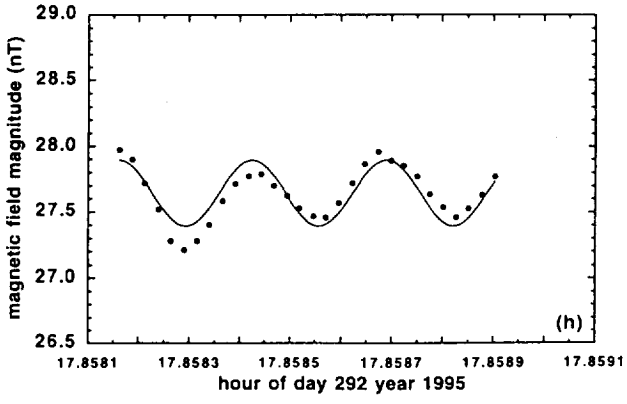
magnetic field magnitude (nT)
29.0
28.5
28.0
27.5
27.0
26.5
17.8581
17.8583
17.8585
17.8587
17.8589
17.8591
hour of day 292 year 1995
(h)

Figure 6

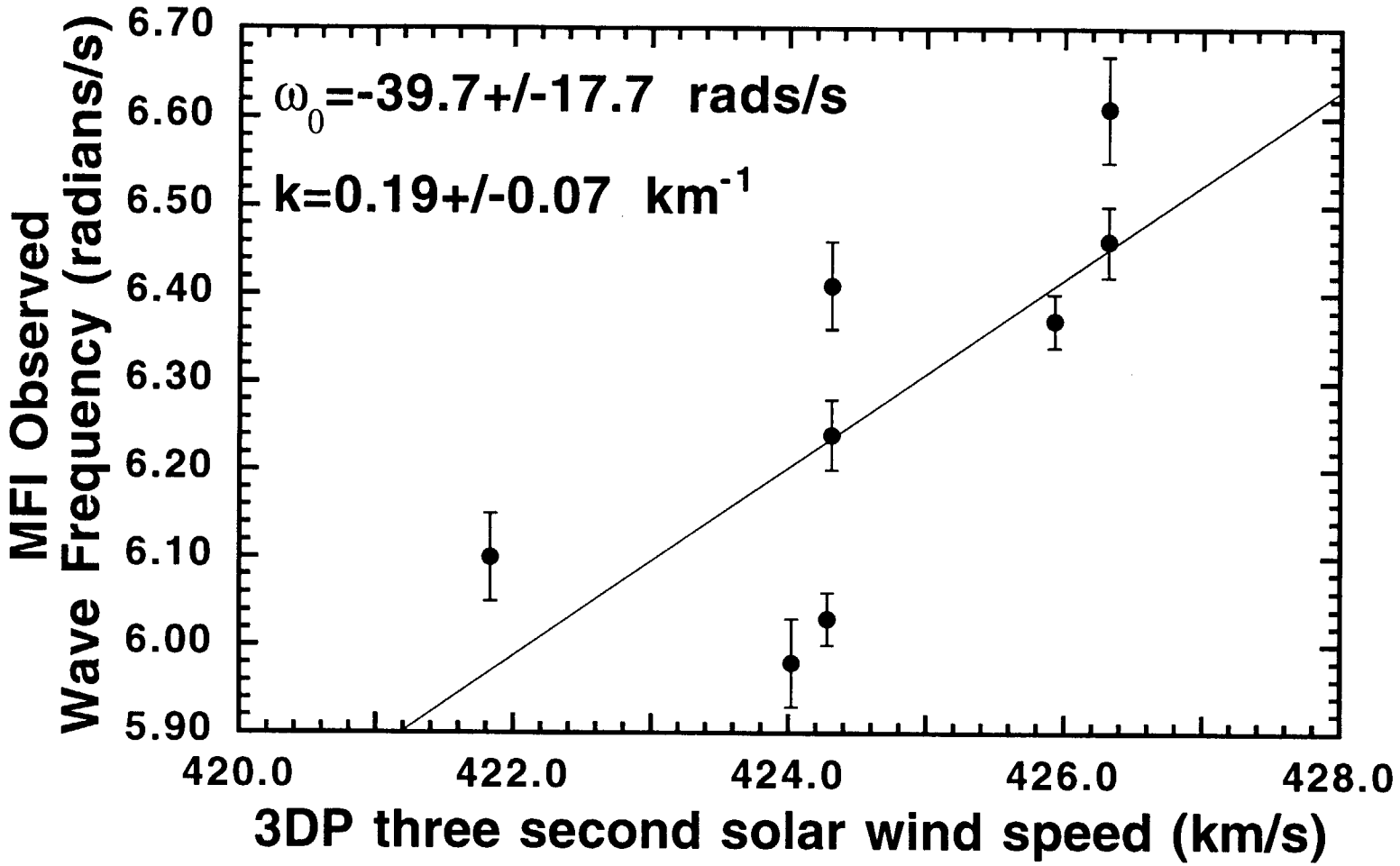
ω_0=-39.7+/-17.7 rads/s
k=0.19+/-0.07 km^{-1}
MFI Observed Wave Frequency (radians/s)
6.70
6.60
6.50
6.40
6.30
6.20
6.10
6.00
5.90
420.0
422.0
424.0
426.0
428.0
3DP three second solar wind speed (km/s)

Figure 7

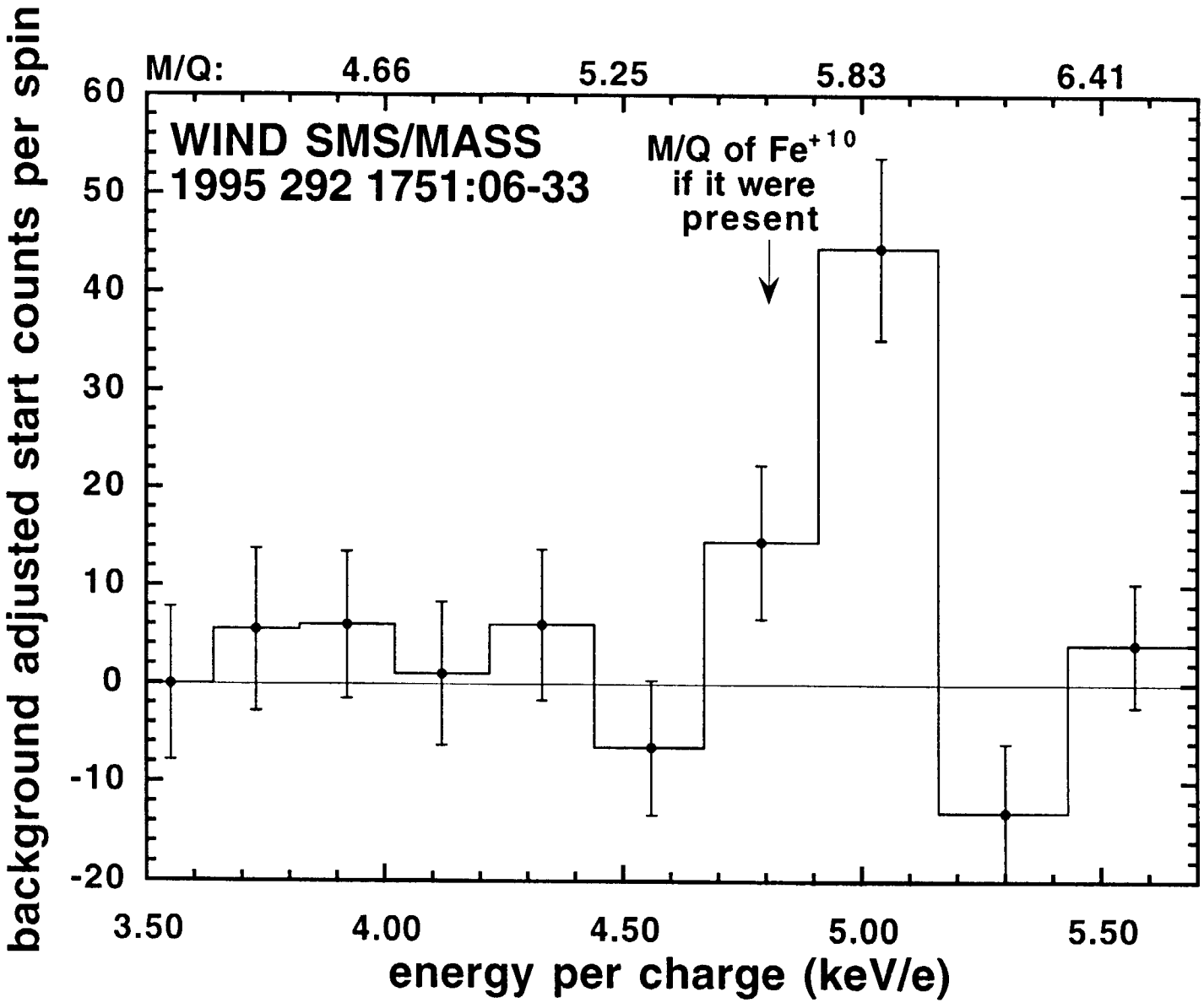
M/Q:
4.66
5.25
5.83
6.41
WIND SMS/MASS
1995 292 1751:06-33
M/Q of Fe+10
if it were
present
60
50
40
30
20
10
0
-10
-20
background adjusted start counts per spin
3.50
4.00
4.50
5.00
5.50
energy per charge (keV/e)

Figure 8

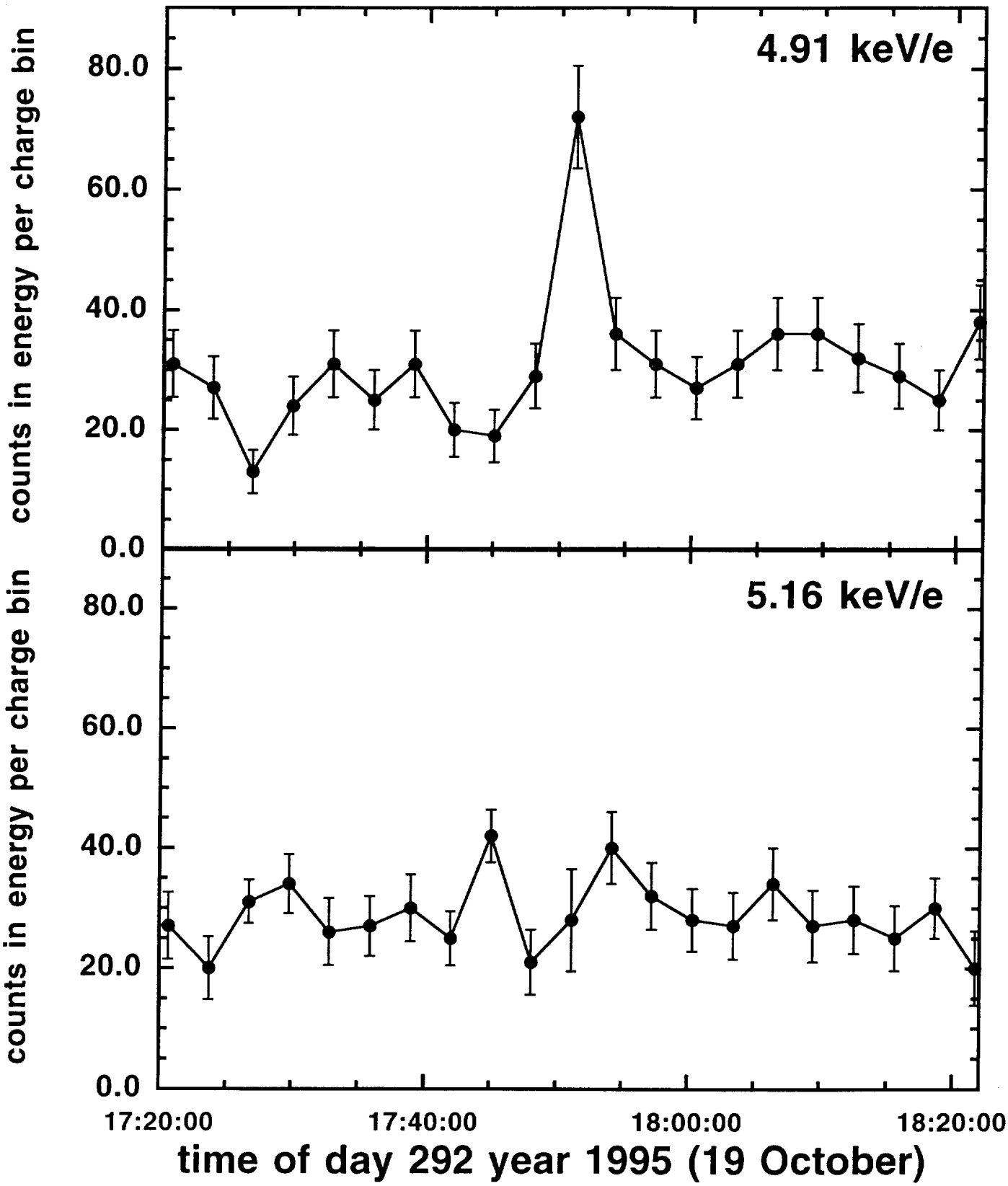
4.91 keV/e
5.16 keV/e
counts in energy per charge bin
counts in energy per charge bin
80.0
60.0
40.0
20.0
0.0
17:20:00
17:40:00
18:00:00
18:20:00
time of day 292 year 1995 (19 October)

Figure 9

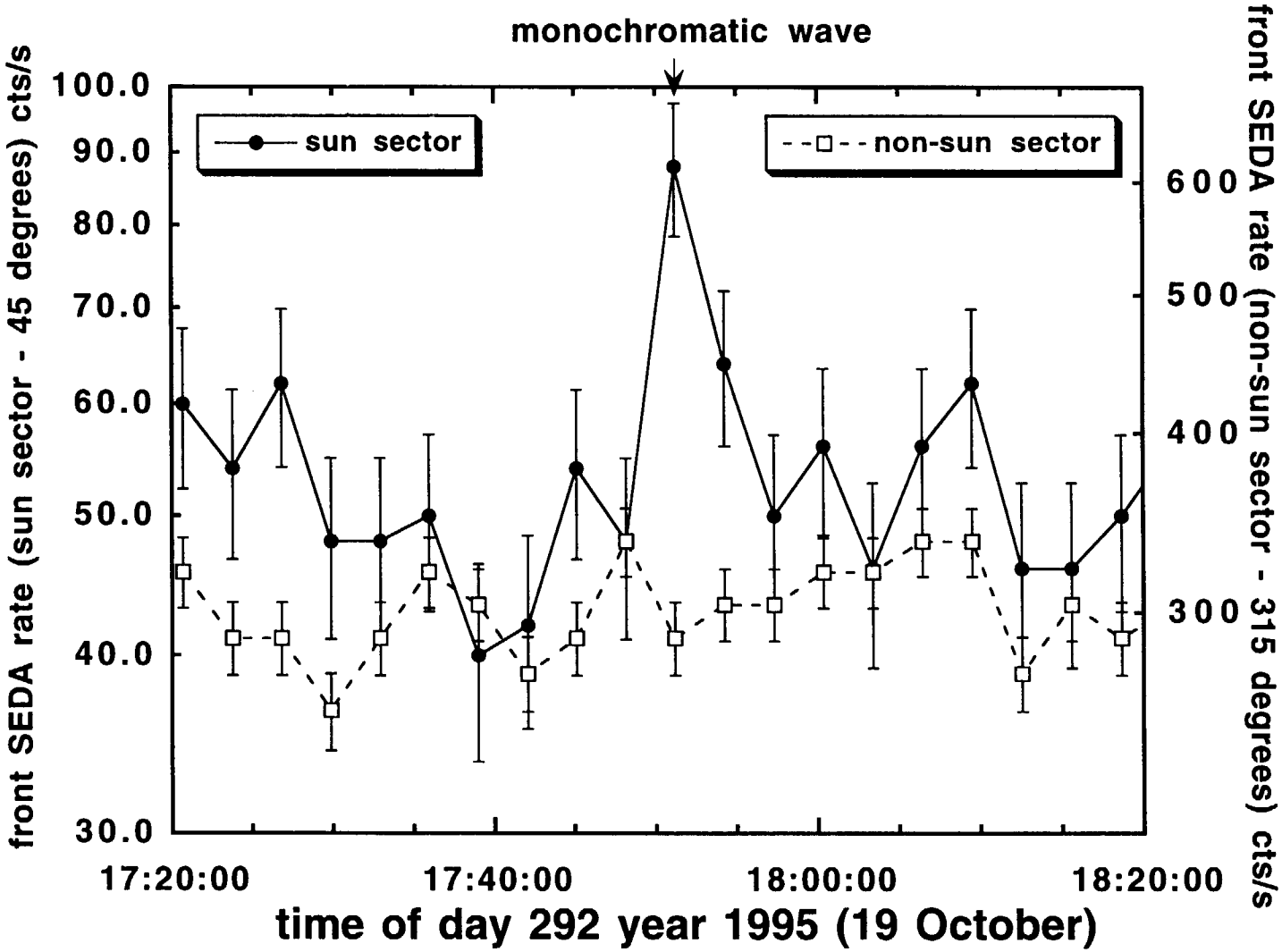
monochromatic wave
sun sector
non-sun sector
front SEDA rate (sun sector - 45 degrees) cts/s
front SEDA rate (non-sun sector - 315 degrees) cts/s
100.0
90.0
80.0
70.0
60.0
50.0
40.0
30.0
600
500
400
300
17:20:00
17:40:00
18:00:00
18:20:00
time of day 292 year 1995 (19 October)

Figure 10

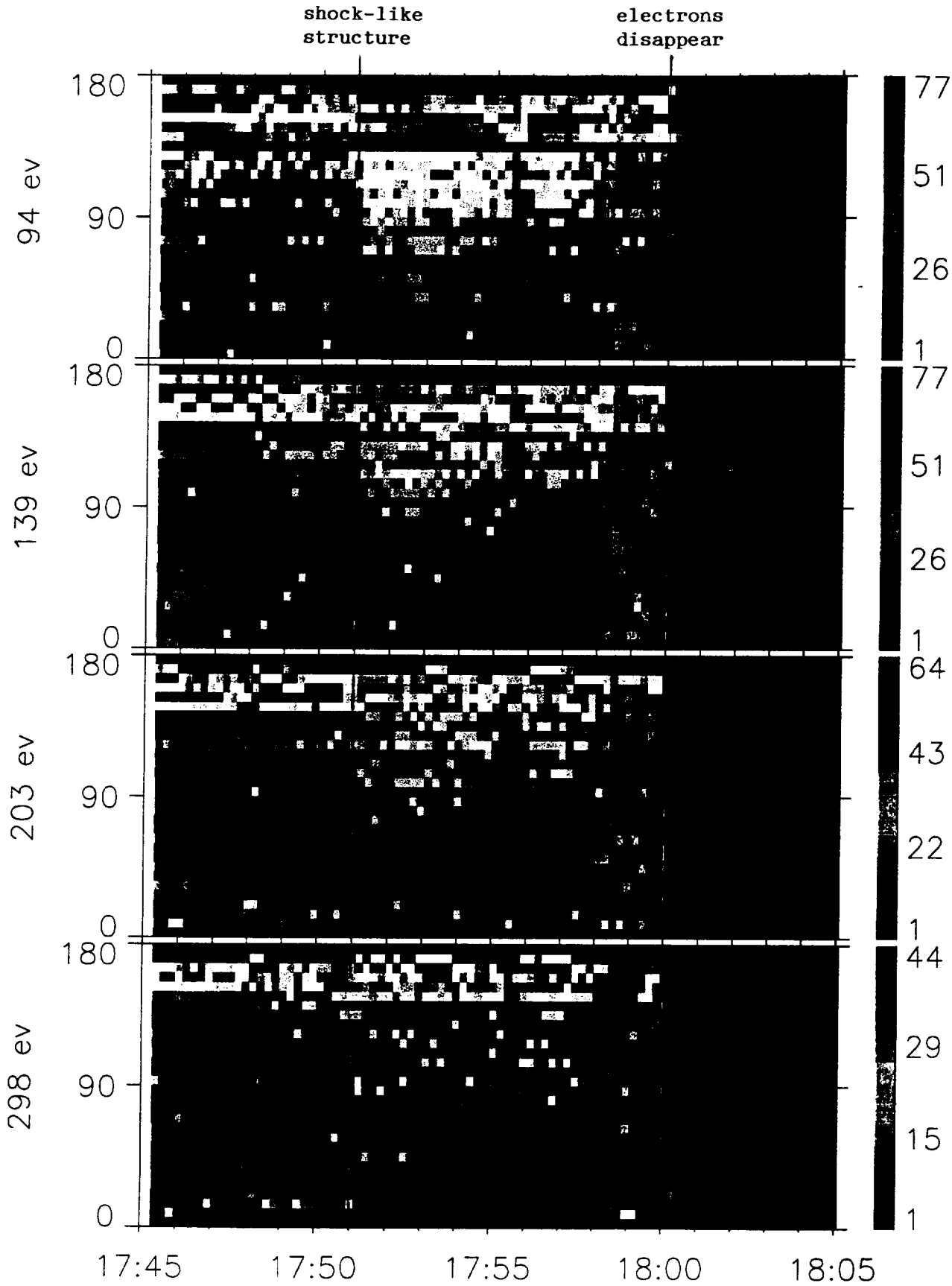
shock-like structure
electrons disappear
94 ev
139 ev
203 ev
298 ev
180
90
0
77
51
26
1
64
43
22
44
29
15
17:45
17:50
17:55
18:00
18:05
19 October 1995
(day 292)

Figure 11

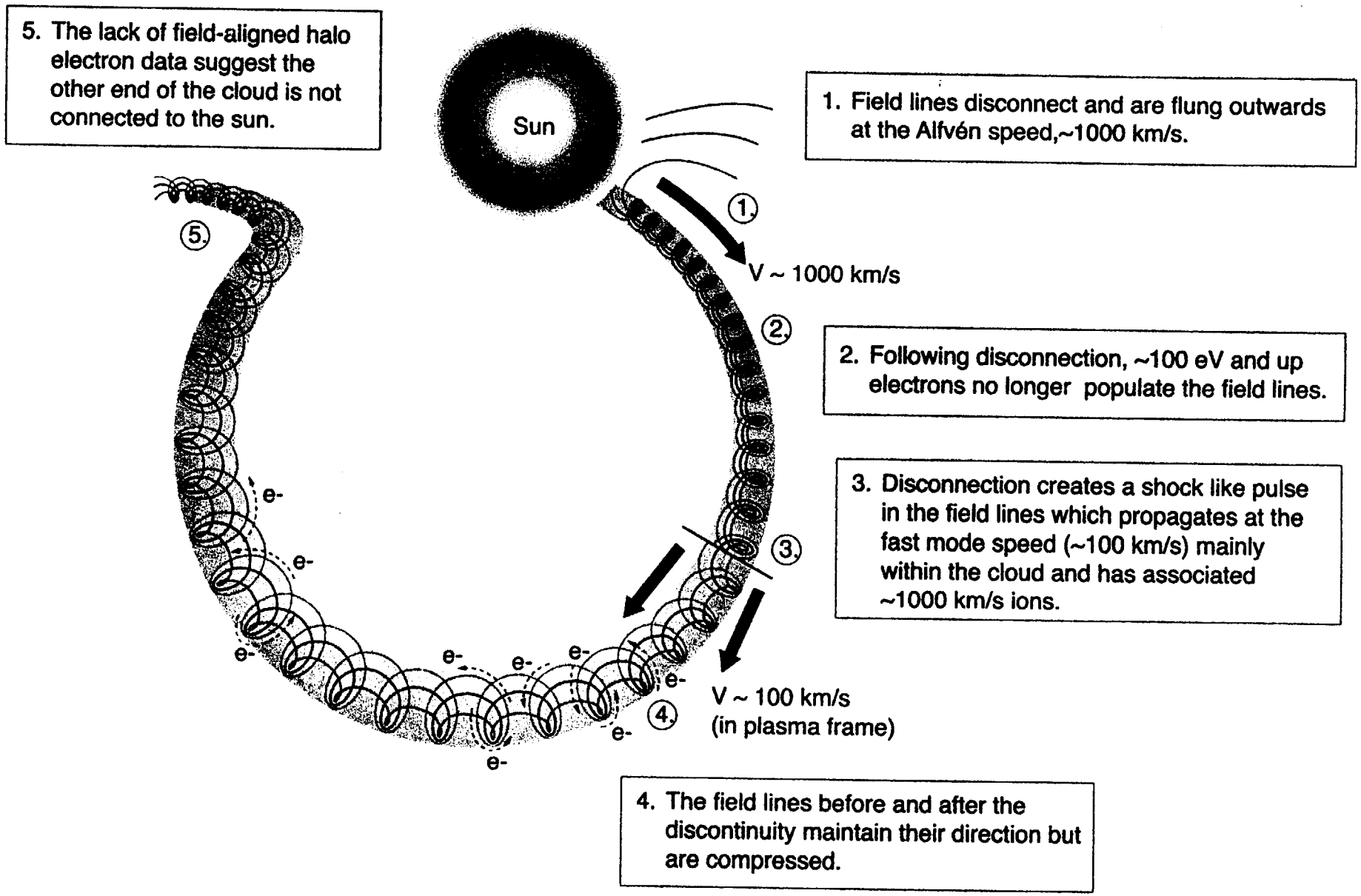

A1519.001

Figure 12

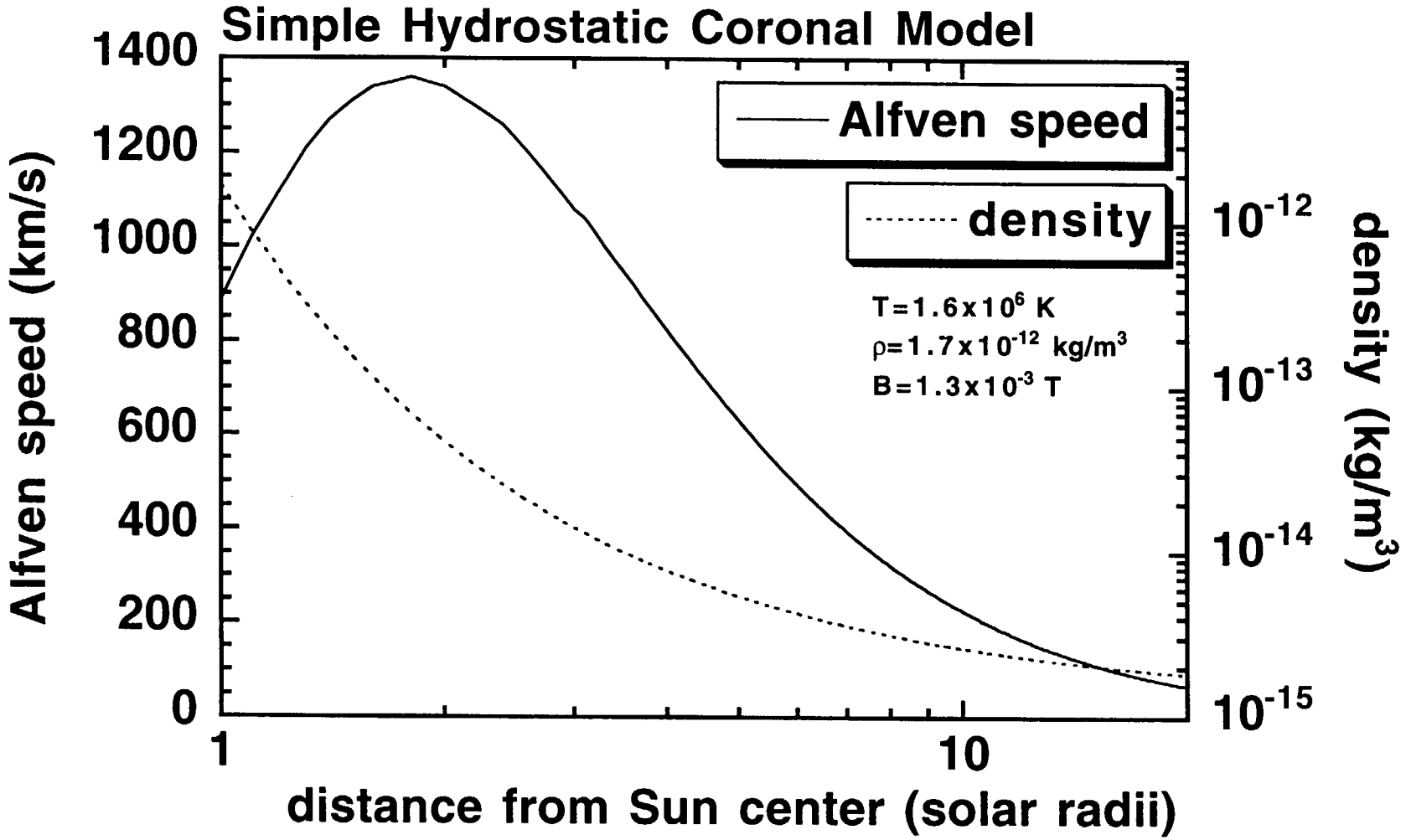
Simple Hydrostatic Coronal Model
Alfven speed
density
T=1.6x10^6 K
ρ=1.7x10^-12 kg/m^3
B=1.3x10^-3 T
Alfven speed (km/s)
density (kg/m^3)
1400
1200
1000
800
600
400
200
0
10^-12
10^-13
10^-14
10^-15
1
10
distance from Sun center (solar radii)

Figure 13